Biogeosciences

Variation in brachiopod microstructure and isotope geochemistry under low-pH–ocean acidification conditions

Facheng Ye[1], **Hana Jurikova**[2], **Lucia Angiolini**[1], **Uwe Brand**[3], **Gaia Crippa**[1], **Daniela Henkel**[2], **Jürgen Laudien**[4], **Claas Hiebenthal**[2], **and Danijela Šmajgl**[5]

[1]Università degli Studi di Milano, Dipartimento di Scienze della Terra "A. Desio", Milan, 20133, Italy
[2]GEOMAR Helmholtz-Zentrum für Ozeanforschung Kiel, 24148 Kiel, Germany
[3]Department of Earth Sciences, Brock University, St. Catharines, Ontario L2S 3A1, Canada
[4]Alfred-Wegener-Institut Helmholtz-Zentrum für Polar- und Meeresforschung, 27515 Bremerhaven, Germany
[5]ThermoFisher Scientific, Hanna-Kunath-Str. 11, 28199 Bremen, Germany

Correspondence: Facheng Ye (facheng.ye@unimi.it)

Abstract. In the last few decades and in the near future CO_2-induced ocean acidification is potentially a big threat to marine calcite-shelled animals (e.g. brachiopods, bivalves, corals and gastropods). Despite the great number of studies focusing on the effects of acidification on shell growth, metabolism, shell dissolution and shell repair, the consequences for biomineral formation remain poorly understood. Only a few studies have addressed the impact of ocean acidification on shell microstructure and geochemistry. In this study, a detailed microstructure and stable isotope geochemistry investigation was performed on nine adult brachiopod specimens of *Magellania venosa* (Dixon, 1789). These were grown in the natural environment as well as in controlled culturing experiments under different pH conditions (ranging from 7.35 to 8.15 ± 0.05) over different time intervals (214 to 335 days). Details of shell microstructural features, such as thickness of the primary layer, density and size of endopunctae and morphology of the basic structural unit of the secondary layer were analysed using scanning electron microscopy. Stable isotope compositions ($\delta^{13}C$ and $\delta^{18}O$) were tested from the secondary shell layer along shell ontogenetic increments in both dorsal and ventral valves. Based on our comprehensive dataset, we observed that, under low-pH conditions, *M. venosa* produced a more organic-rich shell with higher density of and larger endopunctae, and smaller secondary layer fibres. Also, increasingly negative $\delta^{13}C$ and $\delta^{18}O$ values are recorded by the shell produced during culturing and are related to the CO_2 source in the culture set-up. Both the microstructural changes and the stable isotope results are similar to observations on brachiopods from the fossil record and strongly support the value of brachiopods as robust archives of proxies for studying ocean acidification events in the geologic past.

1 Introduction

Since the industrial revolution the surface ocean pH has dropped by 0.1 units and is predicted to drop another 0.3–0.5 units by 2100 (Caldeira and Wickett, 2005; Orr et al., 2005; IPCC, 2013). This is due to the increasing amount of atmospheric carbon dioxide (CO_2) absorbed by the ocean that extensively affects seawater carbonate chemistry (e.g. Caldeira and Wickett, 2003, 2005; Orr et al., 2005; Feely et al., 2004). Increased concentrations of anthropogenic CO_2 are reflected in an elevated concentration of hydrogen ions, which lowers the pH and the availability of carbonate ions. Effects on marine organisms are of great scientific interest for understanding the geological past and the consequences in the immediate future (e.g. Ries et al., 2009), since the decrease in calcium carbonate saturation potentially threatens marine organisms forming biogenic calcium carbonate (e.g. Orr et al., 2005; Guinott et al., 2006; McCulloch et al., 2012; Jantzen et al., 2013a, b). This applies to calcium carbonate shell-forming species, such as brachiopods and mollusks, because they are considered excellent archives documenting

changes in environmental conditions affecting marine organisms (e.g. Kurihara, 2008; Comeau et al., 2009; Hahn et al., 2012, 2014; Watson et al., 2012; Cross et al., 2015, 2016, 2018; Crippa et al., 2016a; Milano et al., 2016; Garbelli et al., 2017; Jurikova et al., 2019).

Recently, several experiments were performed to investigate whether a change in seawater pH may affect growth rate, shell repair and oxygen consumption of calcifying organisms, and how they respond, in general, to ocean acidification (Supplement Table S1). However, despite the great number of studies, the consequences for biomineral formation remain not well understood, as most studies focused mainly on growth, metabolic rates, shell dissolution and shell repair (Table S1, and references therein). Only a few studies deal with the effect of acidification on microstructure (Beniash et al., 2010; Hahn et al., 2012; Stemmer et al., 2013; Fitzer et al., 2014a, b; Milano et al., 2016), and most of them focused on bivalves and show that neither microstructure nor shell hardness seem to be affected by seawater pH.

The few studies that examined brachiopods or brachiopod shells suggest that the latter suffered increased dissolution under lower seawater pH. In other studies, the organism either exhibited no changes or an increase in shell density (calculated as dry mass of the shell (g)/shell volume (cm^3)), but otherwise no changes in shell morphology and trace chemistry (Table 1). Cross et al. (2018) found that punctae became narrower over the past 120 years, which partially explained the increase in shell density over this period. Overall, there appears to be little to no apparent effect on brachiopod morphology or chemistry with lower seawater pH (Cross et al., 2015, 2016, 2018).

Brachiopods possess a low-magnesium calcite shell, which should be more resistant compared to the more soluble forms of $CaCO_3$ such as aragonite and high-Mg calcite (Brand and Veizer, 1980; Morse et al., 2007). The shell microstructure of Rhynchonelliformean brachiopods has been used as a powerful tool to understand the biomineral's response to modern global ocean acidification and similar events in the geologic past (Payne and Clapham, 2012; Cross et al., 2015, 2016; Garbelli et al., 2017). A comprehensive study focusing on fossil brachiopods during the end-Permian mass extinction showed that brachiopods produce shells with increased organic matter content during ocean acidification events (Garbelli et al., 2017).

Here, we describe the microstructure and carbon and oxygen isotopic composition of brachiopod shells belonging to the cold–temperate water species *Magellania venosa* (Dixon, 1789) grown in natural environments as well as under pH-controlled culturing conditions. *M. venosa* represents the largest recent brachiopod species, is often locally abundant (e.g. in Chile; Försterra et al., 2008), and has the highest growth rate recorded for recent brachiopods (Baumgarten et al., 2014). Its low-magnesium calcite shell consists of a microgranular primary layer and a fibrous secondary layer (Smirnova et al., 1991; Baumgarten et al., 2014; Casella et

al., 2018; Romanin et al., 2018) crossed by perforations – endopunctae.

Since little is known about the microstructural and geochemical responses of brachiopods to increased ocean acidification, the main goal of this study is to document any changes in this highly important archival marine organism. We will describe whether and how shell microstructural features such as the primary layer thickness, density of endopunctae and fibre morphology, together with their stable carbon ($\delta^{13}C$) and oxygen ($\delta^{18}O$) isotope compositions, respond to low seawater pH conditions.

2   Materials and methods

2.1   Brachiopod samples and culturing set-up

A full description of the brachiopod sampling and culturing procedure is provided in Jurikova et al. (2019), but we provide an abbreviated version and reiterate the key points. Nine adult individuals of *M. venosa* (Dixon, 1789) were chosen for microstructure investigation and evaluation of their $\delta^{13}C$ and $\delta^{18}O$ values. All specimens were collected by scientific SCUBA divers alive from 20 m water depth of Comau Fjord (Chile) at different localities (Fig. 1). Specimens no. 158 and no. 223 did not experience any treatment after collection from Comau Fjord. The other specimens, no. 43, no. 63, no. 8004, no. 8005, no. 9004, no. 9005 and no. 9006, were cultured under different pH conditions at either AWI in Bremerhaven or GEOMAR (at KIMOCC – Kiel Marine Organisms Culture Centre) in Kiel, Germany (Tables 2 and 3).

In summary, individuals of *M. venosa* were collected alive in Chile and transported to GEOMAR, Germany, in plastic bags filled with seawater, and maintained under controlled conditions in a climate laboratory. The brachiopods were first acclimatized under control conditions for 5 weeks, and prior to the start of the experiment were labelled with a fluorescent dye – calcein (Sigma, CAS 1461–15–0; $50\,mg\,L^{-1}$ for 3 h) (e.g. Baumgarten et al., 2014; Jurikova et al., 2019). As a culture medium we used artificial seawater, which was prepared by mixing a commercial salt with deionized water until the desired salinity and chemical composition were achieved (Atkinson and Bingman, 1998). An overview of the culturing set-up at both laboratories is available in Table 2. Specimens no. 43 and no. 63 were cultured at AWI at pH = 7.66 ($pCO_2 = 1390\,\mu atm$) and pH = 7.44 ($pCO_2 = 2610\,\mu atm$) from 29 August 2013 to 31 March 2014, respectively. Specimens nos. 8004, 8005, 9004, 9005 and 9006 were cultured concurrently at GEOMAR under control or low-pH conditions. Specimens no. 8004 and no. 8005 were maintained under pH settings of 8.0–8.15 from 4 August 2016 to 5 July 2017, conditions similar to those of their fjord habitat. In contrast, specimens nos. 9004, 9005 and 9006 were cultured under low-pH artificial seawater conditions. Low-pH

Table 1. Culturing, dissolution experiments and natural variation on several brachiopod species and shells.

Species / n (number of sample)	Growth parameters	Shell pair/microstructure/oxygen consumption/dissolution of shell/microstructure	Method and material	Environment/conditions T: temperature (°C) S: salinity (PSU) $p\mathrm{CO}_2$ (µatm)	Duration of experiment	Source
Calloria inconspicua (Sowerby, 1846) $n = 123$	(1) > 3 mm in length undamaged individuals were not affected by lower pH; (2) < 3 mm in length undamaged individuals grew faster at pH 7.62 than the control conditions	Shell growth rates and shell repair frequencies were not affected by low pH (>80 % of all damaged individuals repaired after 12 weeks)	Culture experiment	(a) pH 8.16, T 16.5, S 33.9, $p\mathrm{CO}_2$ 465, $\Omega_{\mathrm{calcite}}$ 3.5 (b) pH 7.79, T 16.9, S 33.9, $p\mathrm{CO}_2$ 1130, $\Omega_{\mathrm{calcite}}$ 1.6 (c) pH 7.62, T 16.6, S 33.9, $p\mathrm{CO}_2$ 1536, $\Omega_{\mathrm{calcite}}$ 1.3	12 weeks	Cross et al. (2016)
Calloria inconspicua (Sowerby, 1846) $n_{\mathrm{adult}} = 389$ for shell morphology analyses*		Punctae width decreased by 8.26 %, shell density increased by 3.43 %, no change in shell morphology, punctae density, shell thickness, and shell elemental composition (Ca, Mg, Na, Sr and P) No changes were found in shell dissolution over the last 120 years.	Collected every decade from one locality	Last 2 decades pH reduced 0.1 unit Temperature varied from 10.7 to 13.0 °C $p\mathrm{CO}_2$ varied from 320 to 400 Salinity and $\Omega_{\mathrm{calcite}}$ not provided	120-year record	Cross et al. (2018)
Liothyrella uva (Broderip, 1833) $n = 156$	Not affected by lower pH and temperature	Shell repair frequencies were not affected by low pH and temperature (>83 % of individuals repaired after 7 months)	Culture experiment	(a) pH 7.98, T − 0.3, S 35, $p\mathrm{CO}_2$ 417, $\Omega_{\mathrm{calcite}}$ 1.20 (b) pH 8.05, T 1.7, S 35, $p\mathrm{CO}_2$ 365, $\Omega_{\mathrm{calcite}}$ 1.49 (c) pH 7.75, T 1.9, S 35, $p\mathrm{CO}_2$ 725, $\Omega_{\mathrm{calcite}}$ 0.78 (d) pH 7.54, T 2.2, S 35, $p\mathrm{CO}_2$ 1221, $\Omega_{\mathrm{calcite}}$ 0.50	7 months	Cross et al. (2015)
Liothyrella uva (Broderip, 1833) $n_{\mathrm{post\text{-}mortem}} = 5$	Not applicable	Higher dissolution in gastropods and brachiopods at lower pH after 14 days	Empty shells	(a) pH 7.4, T 4, S 35, $\Omega_{\mathrm{calcite}}$ 0.74 (b) pH 8.2, T 4, S 35, $\Omega_{\mathrm{calcite}}$ 4.22 $p\mathrm{CO}_2$ not provided	14 to 63 days	McClintock et al. (2009)

* A subsample of 40 brachiopods (two to five specimens per decade over the last 120 years) were used for further shell analysis of shell density, punctal width, punctal density, shell dissolution, shell thickness and shell elemental composition.

Table 2. Culture and sensor systems used in *M. venosa* culturing (specimens: no. 43, no. 63, no. 8004, no. 8005, no. 9004, no. 9005 and no. 9006). Operated under controlled experimental settings in climate-controlled laboratories at Alfred-Wegener-Institut Helmholtz-Zentrum für Polar- und Meeresforschung, Bremerhaven, Germany, and at GEOMAR Helmholtz-Zentrum für Ozeanforschung Kiel, Germany.

	Culture system at AWI	Automated sensor systems at AWI	Culture system at GEOMAR	Automated sensor systems at GEOMAR
	Aquarium (150 L/each pH treatment) Supplied from a reservoir tank (twice a week 20 % water was replaced)		Aquarium (150 L/each pH treatment) Supplied from a reservoir tank (twice a month 10 % water was replaced)	
Temperature	Controlled in temperature constant room		Controlled using heaters or coolers	Temperature sensor pond
$p\text{CO}_2$	Bubbling of CO_2	COMPORT, Dennerle, Vinningen; IKS aquastar Aquarium computer V2.xx with Aquapilot 2011	Bubbling of CO_2-enriched air	CONTROS HydroC® underwater CO_2 sensor
Salinity	Mixing Reef commercial sea salt (until October: Aqua Medic, Bissendorf, Germany, thereafter Dupla Marin Reef Salt, Dohse Aquaristik, Grafschaft-Gelsdorf, Germany) with deionized water	Conductivity electrode	Mixing Tropic Marin Pro–Reef commercial sea salt with deionized water	Conductivity electrode
Filtering	Biofilter, protein skimmer and UV sterilizer		Biofilter, protein skimmer and UV sterilizer	
Food	Regularly fed (typically five times per week) with Dupla Rin, Coral Food, Reef Pearls 5–200 μm, alive *Thalassiosira weissflogii,* and 1-day old nauplii of *Artemia salina*		Regularly fed (typically five times per week) with *Rhodomonas baltica*	
Substrate	Sabia Corallina, 7–8 mm, Dohse Aquaristik, Grafschaft-Gelsdorf, Germany		No	

conditions were achieved by bubbling of CO_2 through the tanks at AWI, and by bubbling CO_2-enriched air through the tanks at GEOMAR (Table 2). The acidification experiment at GEOMAR was performed in two phases; the first one from 4 August 2016 to 18 April 2017 during which the $p\text{CO}_2$ was set to 2000 μatm (corresponding to a pH of 7.60), and the second one during which the $p\text{CO}_2$ was set to 4000 μatm (corresponding to a pH of 7.35) from 18 April 2017 to 5 July 2017 (Table 3). In order to distinguish between the shell parts precipitated under the specific pH conditions as well as to allow exact comparison to shells of the control treatment, calcein marking was also carried out prior to the second low-pH experiment of 4000 μatm. Parts of the shell grown under specific pH conditions are indicated in Fig. 2. In addition to the calcein marking, newly grown shell parts may be distinguished from visible growth lines on the surface of the shell (Fig. 2). The total length (maximum distance from the blue line to the anterior margin) of the curved dorsal and ventral valves grown during 11 months of culturing (Fig. 2) varied from < 5 to 15.6 mm (Table 4).

2.2 Microstructural analysis

This study followed the sample preparation method shells suggested by Crippa et al. (2016b). In order to obtain more detailed data on microstructural changes, the samples were cut with a diamond blade along different axes and directions (Fig. 3a). Subsequently, the samples were immersed in 36-volume hydrogen peroxide (H_2O_2) for 24/48 h to remove the organic tissue. The sectioned surfaces were manually smoothed with 1200 grit sandpaper, then quickly (3 s) cleaned with 5 % hydrochloric acid (HCl), immediately washed with water and air-dried. The time of acid etching was kept short so as not to affect the microstructure (Crippa et al., 2016b). Finally, the valve sections were gold-coated

Table 3. Specimens of *M. venosa* sampled from Comau Fjord, Chile, and natural and experimental culturing conditions.

Sample ID	Sample locality at Comau Fjord (Chile)[1]	Sample seawater conditions[2]	Date of collection	Length of ventral valve (mm)	Duration of experiment	Experimental conditions
No. 43	Lilliguapi	pH: $\sim$7.9 T: $\sim$13 S: $\sim$32 D: 20	Feb 2012	37	214 days[3]	pCO$_2$: 1390, pH: 7.66 ± 0.04 T: 11.6 ± 0.5, S: 32.6 Ω_{cal}: 2.0
No. 63	Lilliguapi	pH: $\sim$7.9 T: $\sim$13 S: $\sim$32 D: 20	Feb 2012	23	214 days[3]	pCO$_2$: 2600, pH: 7.44 ± 0.08 T: 11.7 ± 0.5, S: 32.7 Ω_{cal}: 1.4
No. 158	Huinay Dock	pH: $\sim$7.9 T: $\sim$13 S: $\sim$32 D: 20	Dec 2011	36	no	
No. 223	Cahuelmó	pH: $\sim$7.9 T: $\sim$13 S: $\sim$32 D: 23	Feb 2012	30	no	
No. 8004	Comau Fjord	pH: $\sim$7.9 T: $\sim$13 S: $\sim$32 D: 21	Apr 2016	31	335 days[4]	pCO$_2$: 600 pH: 8.00 to 8.15 ± 0.05 T: 10 ± 1, S: 30 Ω_{cal}: 2.0–3.5
No. 8005	Comau Fjord	pH: $\sim$7.9 T: $\sim$13 S: $\sim$32 D: 21	Apr 2016	46	335 days[4]	pCO$_2$: 600 pH: 8.00 to 8.15 ± 0.05 T: 10 ± 1, S: 30 Ω_{cal}: 2.0–3.5
No. 9004	Comau Fjord	pH: $\sim$7.9 T: $\sim$13 S: $\sim$32 D: 21	Apr 2016	41	335 days[4]	pCO$_2$: 2000–4000[5] pH: 7.60 to 7.35 ± 0.05 T: 10 ± 1, S: 30 Ω_{cal}: 0.6–1.1
No. 9005	Comau Fjord	pH: $\sim$7.9 T: $\sim$13 S: $\sim$32 D: 21	Apr 2016	25	335 days[4]	pCO$_2$: 2000–4000[5] pH: 7.60 to 7.35 ± 0.05 T: 10 ± 1, S: 30 Ω_{cal}: 0.6–1.1
No. 9006	Comau Fjord	pH: $\sim$7.9 T: $\sim$13 S: $\sim$32 D: 21	Apr 2016	43	335 days[4]	pCO$_2$: 2000–4000[5] pH: 7.60 to 7.35 ± 0.05 T: 10 ± 1, S: 30 Ω_{cal}: 0.6–1.1

Note: D: depth (m), T: temperature (°C), S: salinity (PSU – practical salinity units), pCO$_2$ (μatm). [1] Cahuelmó 42°15′23′′ S, 72°26′42′′ W, Cross–Huinay 42°23′28′′ S, 72°27′27′′ W, Jetty (Huinay Dock) 42°22′47′′ S, 72°24′56′′ W, Lilliguapi 42°9′43′′ S, 72°35′55′′ W; sample nos. 8004, 8005, 9004, 9005, and 9006 were harvested from three sites in Comau Fjord (Cross-Huinay, Jetty, and Liliguapy), Chile. [2] Reference: Laudien et al. (2014) and Jantzen et al. (2017). [3] Culture experiments conducted at Alfred-Wegener-Institut Helmholtz-Zentrum für Polar- und Meeresforschung, Bremerhaven, Germany. [4] Culture experiments conducted at GEOMAR Helmholtz-Zentrum für Ozeanforschung Kiel, Germany (Jurikova et al., 2019). [5] CO$_2$ concentration was changed during the experiment: to 2000 μatm from 4 August 2016 to 18 April 2017 and to 4000 μatm from 18 April 2017 to 5 July 2017.

**Table 4.** Shell length of specimens of *M. venosa* before and during the culture.

Sample ID	Valve	Initial length before culturing (mm)	New shell growth[a] 257 days (mm)	pH	New shell growth[b] 78 days (mm)	pH
No. 8004	ventral	15.4	14	8.00	1.6	8.15
No. 8005	ventral	40	5	8.00	< 1	8.15
No. 8005	dorsal	36	4	8.00	< 1	8.15
No. 9004	ventral	26.8	13	7.60	1.2	7.35
No. 9005	ventral	11.2	12	7.60	1.8	7.35
No. 9006	ventral	33	9	7.60	< 1	7.35
No. 9006	dorsal	29	8	7.60	< 1	7.35

Note: [a] culturing from 4 August 2016 to 18 April 2017; [b] culturing from 18 April 2017 to 5 July 2017.
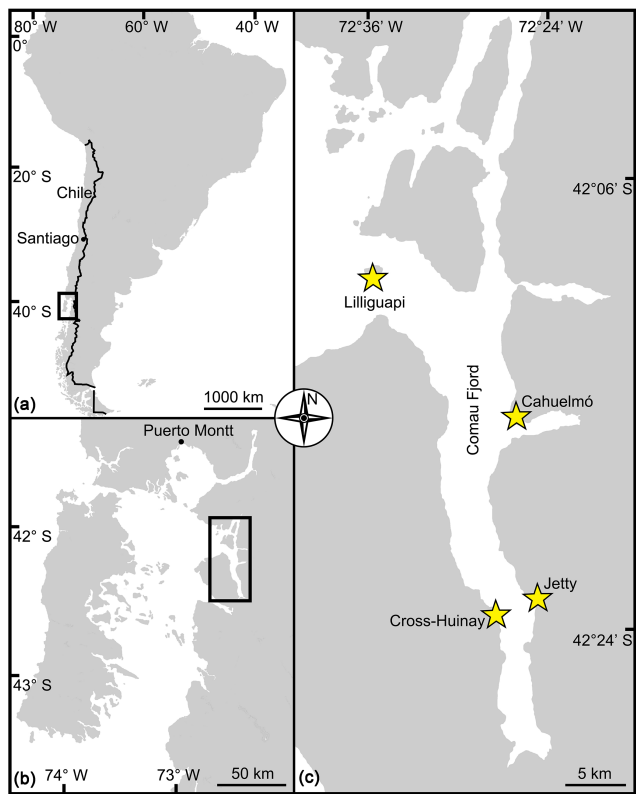
Figure 1. Map of Comau Fjord. **(a)** Overview of Chilean Patagonia. **(b)** Gulf of Ancud with connections in the north and south to the Pacific Ocean. **(c)** Comau Fjord with brachiopod sample collection localities. In both maps the rectangle marks the location of Comau Fjord.

and analysed by a Cambridge S-360 scanning electron microscope with a lanthanum hexaboride (LaB$_6$) source operating at an acceleration voltage of 20 kV (Dipartimento di Scienze della Terra "A. Desio", Università di Milano).
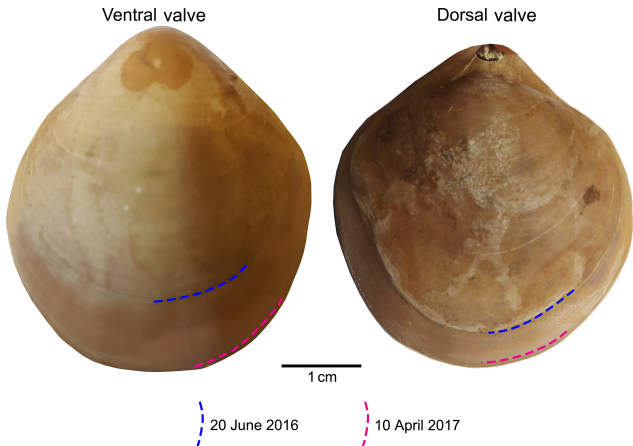
Figure 2. Growth tracked with calcein and marked by blue and red lines on the surface of the brachiopod specimens (no. 9006).
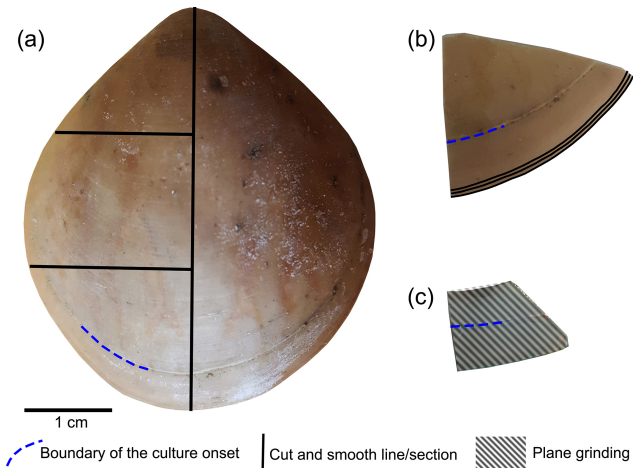
Figure 3. Brachiopod shell sample cut along different axes. **(a)** Longitudinal and transverse sections; **(b)** transverse sections at the anterior margin of the shell; **(c)** plane grinding of the external surface of the shell.

The methods described by Ye et al. (2018a) were followed to investigate the basic microstructural units (fibres) in SEM images. We focused primarily on the anterior margin of the valves, the part that was produced during culturing (hereinafter referred to as *during-culturing*) under different pH conditions. Therefore, additional transverse sections along the growth lines were obtained in the most anterior part (black lines in Fig. 3b) by manually smoothing with 1200 grit sandpaper. Plane grinding was performed on the external surface of the shell (Fig. 3) to investigate the distribution of endopunctae.

The thickness of the primary layer was measured on the SEM images of specimens no. 8005 and no. 9006 (Fig. 4a) in different positions along the longitudinal growth axis (posterior, central and anterior regions). In the vicinity of the transition from natural growth to cultured growth, the region was further subdivided into four sub-zones.

To calculate and measure the density and diameter (max) of endopunctae, squares ($800\,\mu m \times 800\,\mu m$) were located randomly over the smoothed external surface of the anterior shell (Fig. 4b). Four sub-zones (C2, A1, A2, A3) were defined according to their position along the posterior–anterior direction (Fig. 4), while distinguishing the part of the shell produced *before-culturing* and that produced *during-culturing*.

For morphometric analyses, fibres were manually outlined using polygonal lasso in Adobe Photoshop CS6, and size and shape parameters were measured with Image-Pro Plus 6.0 and ImageJ (for convexity). In particular, following Ye et al. (2018a, b) we measured/calculated the Feret diameter (max), area, roundness ($4 area / \pi \times$ Feret diameter (max)^2) and convexity (convex perimeter / perimeter). The width of an individual fibre roughly corresponds to its Max Feret diameter, whereas its height corresponds to the Min Feret diameter (see Fig. 6 in Ye et al., 2018a).

As individual fibres are irregular in shape in the most anterior section of brachiopods, the morphometric measurement method proposed by Ye et al. (2018a, b) is not always suitable. Thus, modifications had to be made to the Ye et al. (2018a, b) measurement method to make the comparative morphometric analysis of the fibres from the anterior part (Fig. 5a, b). First, all SEM images were oriented in the same direction with the base of the primary layer facing upwards. Then a uniformly sized zone ($20\,\mu m \times 20\,\mu m$) was selected for additional measurements with the upper side of the square always placed at the boundary between the primary and secondary layers (Fig. 5c). Two new methods were developed and applied: for Method 1, the width of fibres crossed by two standard lines was measured, which were always located in the same position and at the same distance in all the selected zones (yellow and orange lines in Fig. 5, Method 1). For Method 2, we calculated the number of boundaries based on the number of fibres crossed by the two standard lines (Fig. 5, Method 2). Sub-zones were named according to the following nomenclature: the most anterior transection zone of the ventral valve was named Z1, the second most anterior transection zone of the ventral valve Z2, and so on; the most anterior transection zone of the dorsal valve was named Z4. The standard line facing the primary layer was named "1" and the second standard line "2" (example: "Z1-1" is the sample of the standard line facing the primary layer at the most anterior transect zone of the ventral valve).

## 2.3 Stable isotope analyses of shells

Cleaned shells of specimens nos. 8004, 8005, 9004, 9005 and 9006 were chosen for carbon and oxygen isotope analyses. For specimens no. 8005 and no. 9006, surface contaminants and the primary layer were first manually and then chemically removed by leaching with 10 % HCl, rinsed with distilled water and air-dried. As the primary layer is not secreted in equilibrium with ambient seawater (e.g. Carpenter and Lohmann, 1995; Brand et al., 2003, 2013), it is important to chemically remove it in order to avoid cross-contamination of results. Individual growth increments exclusively come from the secondary layer, and were separated from the shell in both dorsal and ventral valves using a WECHEER (WE 248) microdrill at low speed with a tungsten–carbide milling bit. Shell increment fragments, of similar width, were then powdered using an agate mortar and pestle. For carbon and oxygen isotope analyses about $250\,\mu g$ of powdered calcite of each sample was analysed using an automated carbonate preparation device (GasBench II) connected to a Delta V Advantage (Thermo Fisher Scientific Inc.) isotopic ratio mass spectrometer at the Earth Sciences Department, University of Milan, Italy. The carbon and oxygen isotope compositions are expressed in the conventional delta notation calibrated to the Vienna Pee-Dee Belemnite (V-PDB) scale by the international standards IAEA 603 (International Atomic Energy Agency 603; δ^{18}O: $-2.37 \pm 0.04\,\%_o$, δ^{13}C: $+2.46 \pm 0.01\,\%_o$) and NBS 18 (δ^{18}O: $-23.2 \pm 0.1\,\%_o$, δ^{13}C: $-5.014 \pm 0.035\,\%_o$). Analytical reproducibility (1σ) for these analyses was better than $\pm 0.04\,\%_o$ for δ^{13}C and $\pm 0.1\,\%_o$ for δ^{18}O (Appendix A). Another set of shells, no. 8004, no. 9004 and no. 9005, were gently rinsed with ultra pure water (Milli-Q) and dried for a few days on a hotplate at $40\,°C$ in a clean flow hood. Targeted parts of the shell were sampled for powder under binoculars using a precision drill (Proxxon) with a mounted dental tip. Stable isotope analyses of powders of these specimens were performed at GEOMAR, Kiel, on a Thermo Finnigan MAT 252 mass spectrometer coupled online to an automated Kiel carbonate preparation line. The external reproducibility (1σ) of in-house carbonate standards was better than $\pm 0.1\,\%_o$ and $\pm 0.08\,\%_o$ for δ^{13}C and δ^{18}O, respectively (Appendix A).

2.4 Stable isotope analyses of water samples

In addition to carbon and oxygen isotope analyses of shells, analyses were also carried out on seawater samples collected
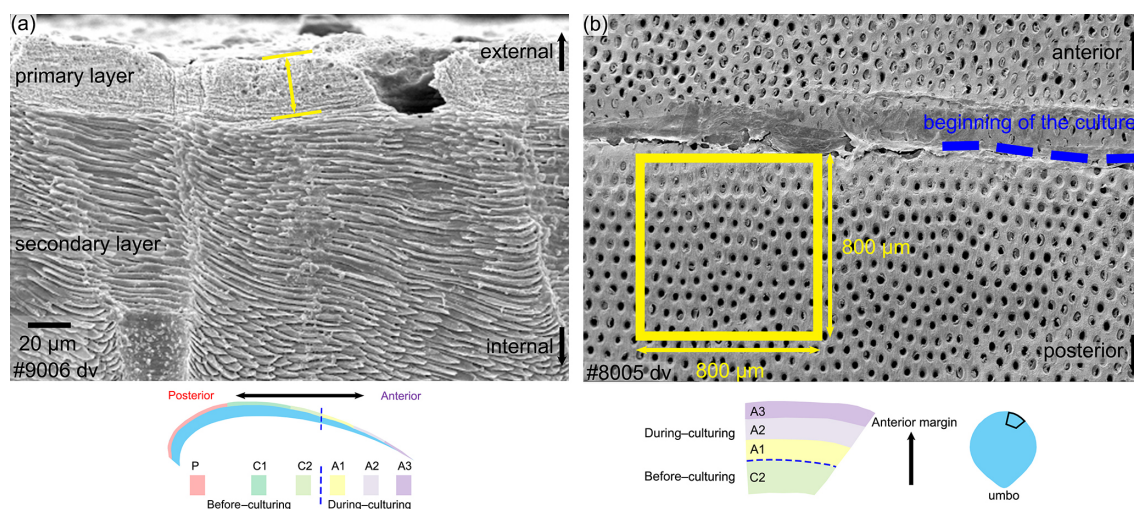
Figure 4. Measurement methods used for the thickness of the primary layer **(a)** and the density of the endopunctae **(b)**. Note that for the latter, endopunctae were counted when included for more than their half-diameter inside the square. dv: dorsal valve.
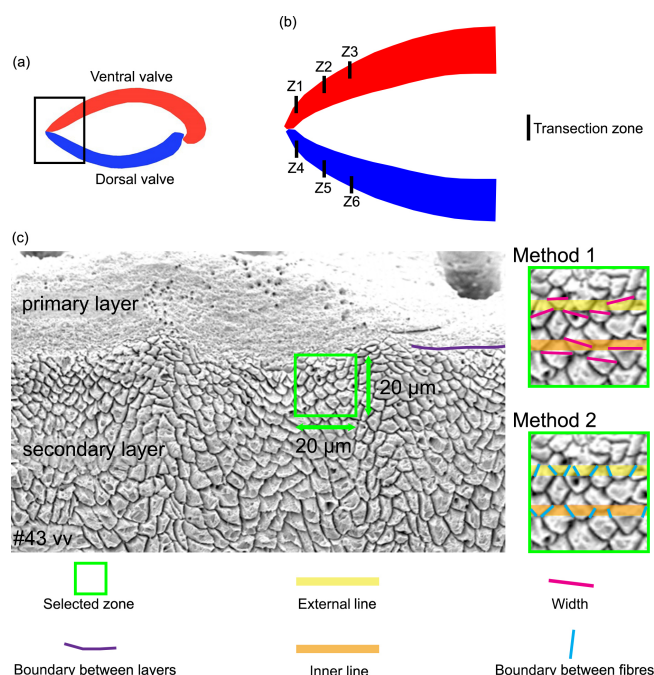
Figure 5. Methods of measurements used in the anterior transverse sections. All SEM images are oriented in the same direction: base of the primary layer facing upwards. A square (20 μm × 20 μm) was analysed with its upper side just overlapping the boundary between the primary and secondary layers. Method 1 refers to the measurement of the width of the fibres crossed by two standard lines, which were located in the same position and at the same distance in all 194 squares (yellow and orange lines); Method 2 involved the calculation of the numbers of boundaries between the fibres that are crossed by two standard lines. vv: ventral valve.

from the culturing tanks. Measurements of $\delta^{13}C_{DIC}$ and $\delta^{18}O_{H_2O}$ were performed using Thermo Scientific™ Delta Ray™ IRIS with URI Connect.

Isotope values ($\delta^{13}C$, $\delta^{18}O$) are reported as per mil (‰) deviations of the isotopic ratios ($^{13}C/^{12}C$, $^{18}O/^{16}O$) calculated to the VPDB scale for $\delta^{13}C$ and VSMOW scale for $\delta^{18}O$ values. Analytical reproducibility (1σ) on three aliquots of each water sample was $\leq 0.03‰$ for both $\delta^{13}C$ and $\delta^{18}O$ values (Appendix B).
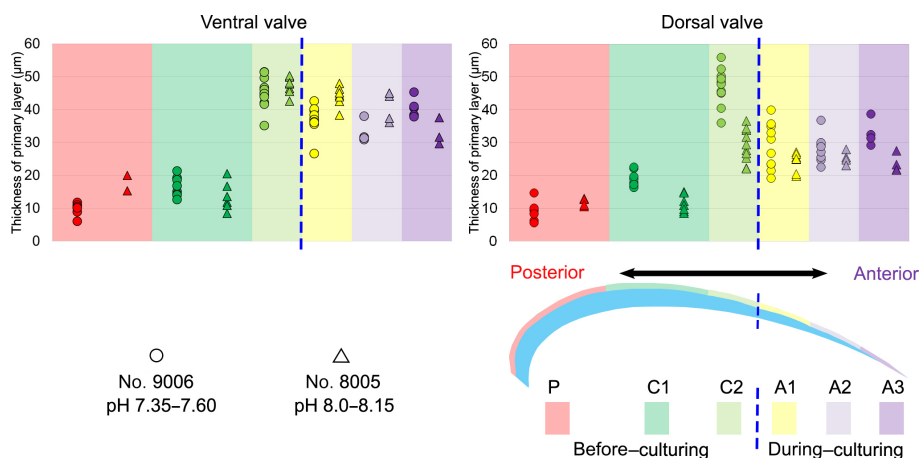
3 Results

3.1 Primary layer thickness

The thickness of the primary layer was measured at different positions along the shell from the posterior (umbonal) region to the *before-culturing* portion and finally to the anterior valve margin (Fig. 6). Generally, in the posterior part of *M. venosa*, the primary layer is missing or it has the lowest recorded thickness. Then, the primary layer progressively thickens toward the central and anterior parts. The thickest primary layer within the same valve is always located just before the beginning of the culture (*before-culturing* portion, Table 5). *During-culturing* the thickness of the primary layer decreases. A most distinct change was observed in specimen no. 9006 cultured at the lowest pH condition of 7.6, and of 7.35 followed by another progressive increase in both valves *during-culturing*. In contrast, the thickness of the primary layer of the control condition specimen (no. 8005) remained stable (dorsal valve) or slightly decreased (Fig. 6, ventral valve; Table 5).

Table 5. Statistical comparison of thickness of the primary layer (µm) along the ontogenetic direction of both valves of specimens no. 8005 and no. 9006 *before-* and *during-culturing*. * Position of zones *before-culturing*: P, C1, C2; *during-culturing*: A1, A2, A3 (cf. Fig. 6). $n =$ number of measurements. Population standard deviation (σ) was calculated using the Excel STDEV.P function. Significant values (p-value ≤ 0.05) are marked in bold. "n/a" stands for not applicable.

Sample	Position*	n	Mean	σ	Min	Max	p values	p values
No. 8005 dorsal	P	4	11.82	1.05	10.55	13.02	P vs. C1 0.755 C1 vs. C2 **< 0.001** C2 vs. A1 **0.033** A1 vs. A2 0.726 A2 vs. A3 n/a	No. 8005DP vs. no.9006DP 0.120
	C1	8	11.40	2.29	8.50	15.05		
	C2	10	28.99	4.79	22.15	36.65		
	A1	8	24.36	2.52	19.80	27.06		
	A2	7	24.83	2.15	21.67	27.94		
	A3	1	21.77	n/a	n/a	n/a		No. 8005DC1 vs. no. 9006DC1 **< 0.001**
No. 8005 ventral	P	2	17.64	2.36	15.28	20	P vs. C1 n/a C1 vs. C2 **< 0.001** C2 vs. A1 **0.028** A1 vs. A2 0.289 A2 vs. A3 **0.017**	No. 8005DC2 vs. no. 9006DC2 **< 0.001**
	C1	6	13.68	3.96	8.50	20.52		No. 8005DA1 vs. no. 9006DA1 0.088
	C2	8	47.57	2.49	42.55	50.27		
	A1	8	44.18	2.68	38.33	47.98		No. 8005DA2 vs. no. 9006DA2 0.101
	A2	6	42.09	3.85	36.06	45.04		No. 8005DA3 vs. no. 9006DA3 n/a
	A3	4	34.09	3.51	29.63	37.52		No. 8005VP vs. no. 9006VP n/a
No. 9006 dorsal	P	7	9.08	2.77	5.56	14.64	P vs. C1 **< 0.001** C1 vs. C2 **< 0.001** C2 vs. A1 **< 0.001** A1 vs. A2 0.779 A2 vs. A3 0.096	No. 8005VC1 vs. no. 9006VC1 0.123
	C1	10	18.78	2.04	16.90	22.50		
	C2	11	46.91	5.22	35.92	55.86		No. 8005VC2 vs. no. 9006VC2 0.194
	A1	10	28.83	6.65	19.04	39.93		No. 8005VA1 vs. no. 9006VA1 **< 0.001**
	A2	8	28.06	4.03	22.50	36.69		
	A3	4	32.84	3.55	29.10	38.65		No. 8005VA2 vs. no. 9006VA2 **0.007**
No. 9006 ventral	P	7	9.78	1.72	6.07	11.79	P vs. C1 **< 0.001** C1 vs. C2 **< 0.001** C2 vs. A1 **< 0.001** A1 vs. A2 0.102 A2 vs. A3 **0.008**	No. 8005VA3 vs. no. 9006VA3 **0.027**
	C1	9	16.75	2.77	12.61	21.29		
	C2	12	45.16	4.34	35.09	51.40		
	A1	11	36.92	3.82	26.62	42.54		
	A2	4	32.95	2.91	30.84	37.95		
	A3	5	40.55	2.63	37.78	45.23		

Figure 6. Variation of the thickness of the primary layer (ventral and dorsal valves) of a *M. venosa* specimen cultured at pH 7.35 and 7.6 (no. 9006) and a specimen cultured at pH 8.0 and 8.15 (no. 8005).

3.2 Endopunctae density and size

On the externally ground surface of the anterior part, the total number and the diameter (max) of endopunctae in a squared area of $800\,\mu m \times 800\,\mu m$ were measured in four *before-culturing* parts and of the *during-culturing* parts of the shell (Fig. 7). Generally, the density of endopunctae gradually increased along the selected transect from ca. 185 to ca. 305 mm^{-2} in the ventral valve and from ca. 220 to ca. 280 mm^{-2} in the dorsal valve (Table 6). The size of en-

Table 6. Statistical comparison of the number of endopunctae (per mm^2) on both valves of no. 8005 and no. 9006. * Position of zones *before-culturing*: C2, and *during-culturing*: A1, A2, A3 (cf. Fig. 7). "n/a" stands for not applicable.

Sample	Zone*	n	Mean	σ	Min	Max
No. 8005 dorsal	C2	3	236	10.4	225	250
	A1	1	280	n/a	n/a	n/a
	A2	2	244	12.5	231	256
	A3	2	281	14.1	267	295
No. 8005 ventral	C2	2	225	1.6	223	227
	A1	1	242	n/a	n/a	n/a
	A2	2	241	5.5	236	247
	A3	2	269	6.3	263	275
No. 9006 dorsal	C2	2	221	8.6	213	230
	A1	1	269	n/a	n/a	n/a
	A2	2	250	3.1	247	253
	A3	2	266	3.1	263	269
No. 9006 ventral	C2	2	186	3.1	183	189
	A1	1	234	n/a	n/a	n/a
	A2	2	230	4.7	225	234
	A3	2	308	1.6	306	309
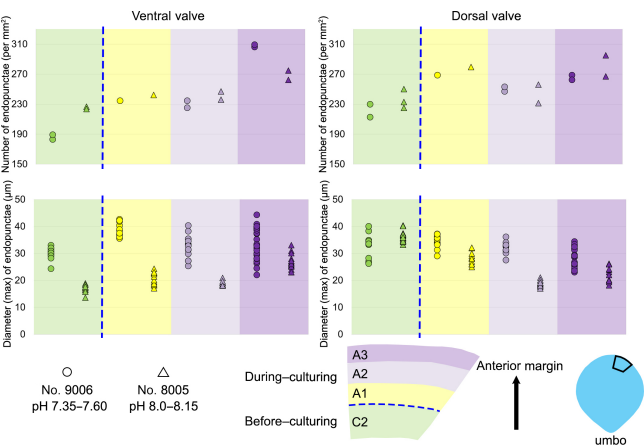
Figure 7. Variation in the number and diameter (max) of endopunctae in the dorsal and ventral valves from a specimen of *M. venosa* cultured at pH 7.35 and 7.6 (no. 9006) and a specimen cultured at pH 8.0 and 8.15 (no. 8005).

dopunctae increased along the selected transect in the ventral valve (from ca. 17 to 33 μm; Table 7), but it slightly decreases in the dorsal valve from ca. 36 μm to ca. 21 μm (Table 7). These density and size trends were observed in both specimens cultured under different pH conditions. However, it is noteworthy that in the most anterior part (*during-culturing*) of the ventral valve of no. 9006 (cultured at a pH of 7.35), the density of endopunctae sharply increases and their diameter reached recorded maximum values (Table 6).
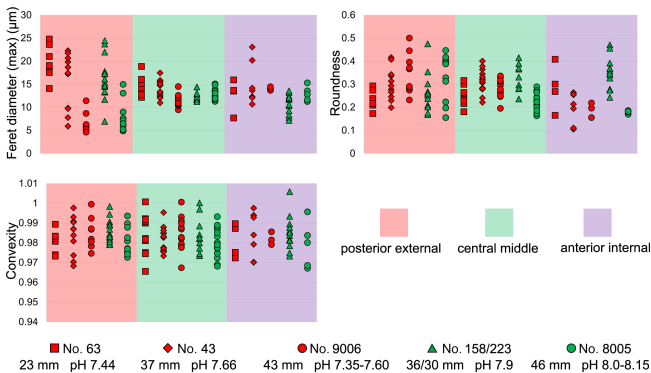
Figure 8. Comparisons of the fibre size and shape of *M. venosa* (ventral and dorsal valves) at different positions along the posterior–anterior axis; pH conditions of culturing or natural environment are reported. One circle point represents one measurement. Outliers have been removed, identified with Tukey's fences (Tukey, 1977) when falling outside fences F1 and F2 (F1 = Q1 − 1.5IQR; F2 = Q3 + 1.5IQR; Q1/Q3: first/third quartiles; IQR (interquartile range): Q3–Q1).

3.3 Shell morphometrics

3.3.1 *Before-culturing*

Ontogenetic variation in fibre morphometry is not obvious when all six adult specimens are considered (Table 8). However, clearer growth trends can be observed when considering the data from each single specimen separately, where t-tests on morphometric data from specimens no. 8005 and no. 9006 show that there are significant differences in Feret diameter (max) and roundness between the posterior and the middle part of the shell (Table 9). Overall, in specimens no. 8005 and no. 9006, fibres become wider from the posterior to mid-shell. In contrast, no. 63 shows an opposite trend along the posterior to mid-shell direction (Fig. 8). The fibre size and shape in the other specimens are rather constant.

3.3.2 *During-culturing*

Transverse sections obtained by smoothing of the anterior part of the shell allowed us to measure the width of 1392 fibres (Max Ferret diameter (max); see in Method 1) and select 388 sub-zones for fibre boundary calculation. In addition, they allowed us to focus on the parts that were produced under the different low-pH treatments (7.66, 7.60, 7.44, and 7.35, respectively).

In all six specimens, the width of fibres increases and the number of boundaries decreases along a transect from the more external sub-zone to the immediately inner sub-zone (e.g. Z1-1 to Z1-2; Z2-1 to Z2-2; and Z3-1 to Z3-2 in Fig. 9a, b, c, d). This means that within a 10 μm distance the sizes of fibres become larger from the exterior part to the interior part of the shell.

Table 7. Statistical comparison of the diameter (max) (µm) of endopunctae on valves of no. 8005 and no. 9006. * Position of zones *before-culturing*: C2, and *during-culturing*: A1, A2, A3 (cf. Fig. 7). Significant values (p-value ≤ 0.05) are marked in bold.

Sample	Zone*	n	Mean	σ	Min	Max	p values	p values
No. 8005D	C2	21	36.04	1.78	33.2	40.4	C2 vs. A1 **< 0.001**	
	A1	10	28.36	2.33	25	32.1	A1 vs. A2 **< 0.001**	
	A2	15	18.77	1.10	17	21.1	A2 vs. A3 **0.001**	No. 8005DC2 vs. no. 9006DC2 **0.025**
	A3	13	21.8	2.53	18.2	26.2		
No. 8005V	C2	11	17.07	1.42	13.6	18.9	C2 vs. A1 **< 0.001**	No. 8005DA1 vs. no. 9006DA1 **< 0.001**
	A1	13	20.88	2.22	17.1	24.3	A1 vs. A2 **0.007**	No. 8005DA2 vs. no. 9006DA2 **< 0.001**
	A2	12	18.74	0.84	18	20.9	A2 vs. A3 **< 0.001**	No. 8005DA3 vs. no. 9006DA3 **< 0.001**
	A3	14	26.83	2.83	23	33.1		
No. 9006D	C2	12	32.54	4.39	26.2	40	C2 vs. A1 0.178	No. 8005VC2 vs. no. 9006VC2 **< 0.001**
	A1	13	34.63	2.33	29	37.2	A1 vs. A2 **0.012**	No. 8005VA1 vs. no. 9006VA1 **< 0.001**
	A2	11	32.02	2.12	27.5	36.1	A2 vs. A3 **0.005**	No. 8005VA2 vs. no. 9006VA2 **< 0.001**
	A3	19	28.75	3.51	23	34.4		
No. 9006V	C2	13	29.98	2.04	24.3	33	C2 vs. A1 **< 0.001**	No. 8005VA3 vs. no. 9006VA3 **< 0.001**
	A1	12	38.66	2.41	35.5	42.6	A1 vs. A2 **< 0.001**	
	A2	14	32.51	4.08	25.3	40.3	A2 vs. A3 0.516	
	A3	24	33.70	5.82	22	44.3		
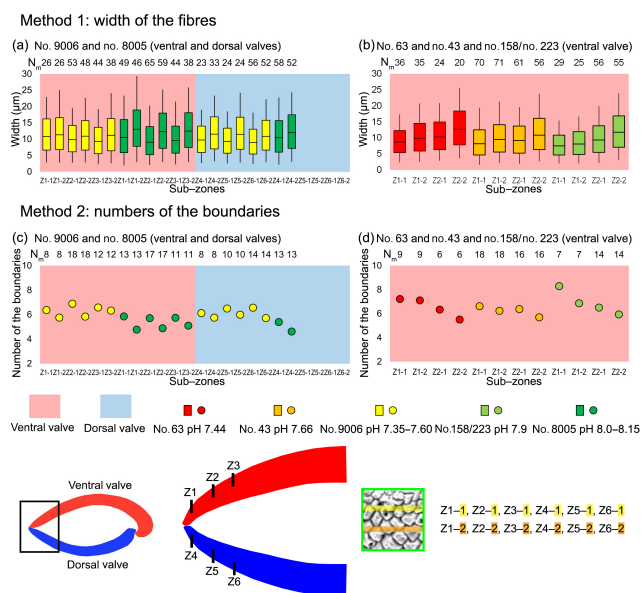
Figure 9. Differences in sizes of fibres of *M. venosa* (ventral and dorsal valves) in the anterior transverse sections of specimens cultured under different pH conditions. **(a, b)** The bottom/top of the box and the band inside the box are the first/third quartiles and the median of the data, respectively; ends of the whiskers represent the minimums and maximums. **(c, d)** Circle point represents average data; N_m: number of measurement.

Results from specimen no. 9006 (pH: 7.60 and 7.35) were compared to those of control specimen no. 8005 (pH: 8.00 and 8.15). Specimen no. 9006 cultured under low-pH conditions (pH: 7.60 and 7.35) had narrower fibres and a higher number of fibre boundaries when compared to those of control specimen no. 8005 (Fig. 9a, c). It is worth noting that, in comparison between the two specimens, the fibres from Z1-2 and Z2-2 of no. 9006 are significantly smaller than those of no. 8005. However, there is no significant difference in the size of fibres from sub-zone Z3-2 between the two specimens (Table 10).

The results from specimens (no. 43 and no. 63) grown under low-pH conditions (pH: 7.66 and 7.44) for a short time interval of 214 days are difficult to interpret, as in this case there is no direct control experiment sample to compare with the cultured specimens (Fig. 9b, d). The specimens grown in the natural environment (no. 158 and no. 223) have different sizes and ages, and so different growth rates may affect the size of the fibres.

3.4 Stable isotopes

The carbon and oxygen isotope compositions were measured along the shell growth increments in the dorsal and ventral valves (Fig. 10). In the *before-culturing* part of the shell, δ^{13}C values varied between -2.02 and $+0.45$ ‰ in control group specimens no. 8004 and no. 8005, whereas they varied between -9.24 and -0.53 ‰ in low-pH group specimens

F. Ye et al.: Variation in brachiopod microstructure and isotope geochemistry

Table 8. Statistical comparison of fibre size and shape of the posterior external vs. central middle parts of the ventral and dorsal valves. NC: non-cultured samples no. 158 and no. 223; CU: cultured samples nos. 43, 63, 8005, and 9006; Vpe: ventral posterior external, Vcm: ventral central middle, Dpe: dorsal posterior external, Dcm: dorsal central middle. Significant values (p-value ≤ 0.05) are marked in bold.

Sample	Position	n	Mean	σ	Min	Max	p-values
Feret diameter (max) (µm):							
NC	Vpe	7	13.79	3.22	6.97	17.33	
CU	Vpe	26	12.47	6.58	4.59	24.78	NC Vpe vs. CU Vpe 0.486
NC	Vcm	32	12.98	2.91	7.09	20.61	NC Vcm vs. CU Vcm 0.633 NC Vpe vs. NC Vcm 0.533
CU	Vcm	65	13.24	2.15	8.68	18.84	CU Vpe vs. CU Vcm 0.572
NC	Dpe	8	18.36	4.22	13.30	24.46	
CU	Dpe	12	10.78	6.36	4.85	22.29	NC Dpe vs. CU Dpe **0.012**
NC	Dcm	12	12.14	1.13	9.84	14.42	NC Dcm vs. CU Dcm 0.373 NC Dpe vs. NC Dcm **0.012**
CU	Dcm	46	12.51	1.57	9.45	15.89	CU Dpe vs. CU Dcm 0.391
Roundness:							
NC	Vpe	7	0.308	0.077	0.239	0.475	
CU	Vpe	26	0.296	0.074	0.172	0.446	NC Vpe vs. CU Vpe 0.717
NC	Vcm	29	0.282	0.051	0.179	0.389	NC Vcm vs. CU Vcm 0.396 NC Vpe vs. NC Vcm 0.296
CU	Vcm	65	0.272	0.051	0.180	0.421	CU Vpe vs. CU Vcm 0.146
NC	Dpe	8	0.220	0.034	0.169	0.268	
CU	Dpe	12	0.337	0.100	0.155	0.500	NC Dpe vs. CU Dpe **0.003**
NC	Dcm	11	0.311	0.068	0.192	0.416	NC Dcm vs. CU Dcm **0.028** NC Dpe vs. NC Dcm **0.005**
CU	Dcm	48	0.269	0.051	0.162	0.378	CU Dpe vs. CU Dcm **0.048**
Convexity:							
NC	Vpe	7	0.985	0.004	0.979	0.991	
CU	Vpe	26	0.982	0.008	0.968	0.999	NC Vpe vs. CU Vpe 0.309
NC	Vcm	32	0.984	0.005	0.975	1.000	NC Vcm vs. CU Vcm 0.655 NC Vpe vs. NC Vcm 0.823
CU	Vcm	62	0.984	0.008	0.965	1.008	CU Vpe vs. CU Vcm 0.257
NC	Dpe	8	0.987	0.006	0.979	0.998	
CU	Dpe	11	0.985	0.007	0.973	0.998	NC Dpe vs. CU Dpe 0.604
NC	Dcm	12	0.984	0.008	0.973	1.000	NC Dcm vs. CU Dcm 0.273 NC Dpe vs. NC Dcm 0.543
CU	Dcm	48	0.982	0.008	0.967	1.001	CU Dpe vs. CU Dcm 0.207

nos. 9004, 9005 and 9006. Similarly, in the *before-culturing* shell part, δ^{18}O values varied between -2.39 and $+0.21$ ‰ in control group specimens no. 8004 and no. 8005, but varied between -4.92 ‰ and $+0.05$ ‰ in low-pH group specimens nos. 9004, 9005 and 9006.

In the *during-culturing* part, δ^{13}C values varied between -6.80 and -1.34 ‰ in control group specimens no. 8004 and no. 8005, whereas they varied between -27.09 ‰ and -9.69 ‰ in low-pH group specimens nos. 9004, 9005 and

9006 (Fig. 10). Concomitantly, δ^{18}O values varied between -6.80 ‰ and -1.34 ‰ in control group specimens no. 8004 and no. 8005, but varied between -6.97 ‰ and -5.29 ‰ in low-pH group specimens nos. 9004, 9005 and 9006 (Fig. 10).

A marked drop in δ^{13}C and δ^{18}O is recorded in the shell increments produced *during-culturing*, particularly so in the specimens grown under low-pH conditions of 7.60 and 7.35, where δ^{13}C values decreased to -27.09 ‰ (Fig. 10).

Biogeosciences, 16, 617–642, 2019

www.biogeosciences.net/16/617/2019/

Table 9. Statistical comparison of fibre size and shape data of the posterior external vs. central middle area for no. 8005 and no. 9006, considering both valves together. pe: posterior external; cm: central middle. Significant values (p-value ≤ 0.05) are marked in bold.

Sample	Position	n	Mean	σ	Min	Max	p-values
Feret diameter (max) (μm)							
No. 8005	pe	10	7.92	3.30	4.85	14.97	
No. 8005	cm	36	12.29	1.64	9.63	15.89	No. 8005 pe vs. no.9006 pe 0.265 No. 8005 cm vs. no.9006 cm 0.171
No. 9006	pe	10	6.45	1.95	4.59	11.41	No. 8005 pe vs. no.8005 cm **0.003** No. 9006 pe vs. no.9006 cm **< 0.001**
No. 9006	cm	25	11.73	1.39	8.68	15.24	
Roundness							
No. 8005	pe	10	0.33	0.097	0.155	0.446	
No. 8005	cm	36	0.25	0.045	0.162	0.374	No. 8005 pe vs. no.9006 pe 0.547 No. 8005 cm vs. no.9006 cm **0.012**
No. 9006	pe	10	0.35	0.079	0.232	0.500	No. 8005 pe vs. no.8005 cm **0.040** No. 9006 pe vs. no.9006 cm **0.022**
No. 9006	cm	26	0.28	0.043	0.195	0.369	
Convexity							
No. 8005	pe	10	0.981	0.007	0.973	0.994	
No. 8005	cm	35	0.982	0.008	0.968	1.001	No. 8005 pe vs. no.9006 pe 0.308 No. 8005 cm vs. no.9006 cm 0.277
No. 9006	pe	9	0.985	0.007	0.975	0.999	No. 8005 pe vs. no.8005 cm 0.829 No. 9006 pe vs. no.9006 cm 0.775
No. 9006	cm	26	0.984	0.007	0.967	1.001	
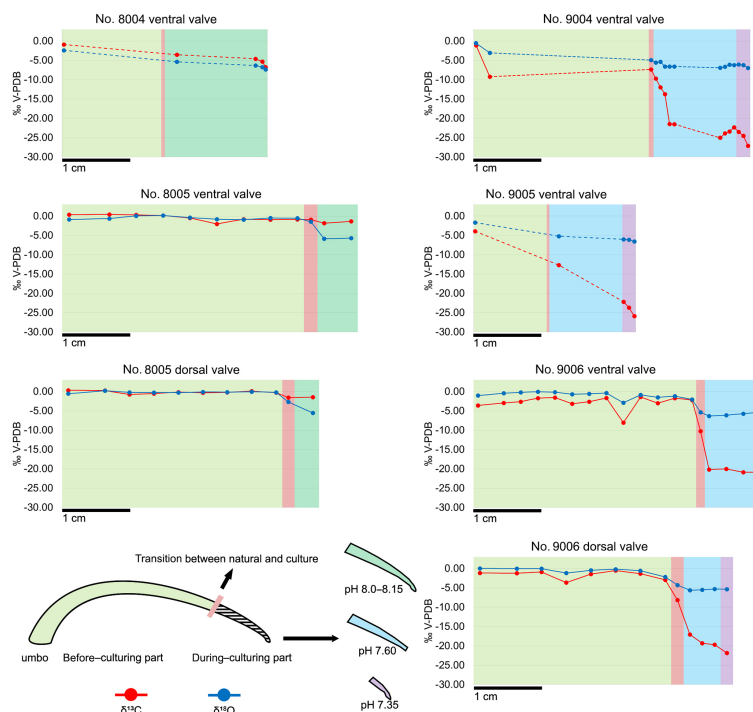
Figure 10. Plots of δ^{13}C and δ^{18}O of the ventral and dorsal valves of *M. venosa* specimens along their growth axis. Different colour backgrounds represent different pH conditions during growth. When few data were available, data points were joined by dashed lines.

Table 10. Statistical comparison of fibre sizes of *M. venosa* (ventral and dorsal valve) in the anterior transverse sections (*during-culturing*). * For the position of zones (Z1-1, Z2-1, Z3-1, Z1-2, Z2-2, Z3-2, Z4-1, Z5-1, Z4-2, Z5-2), see Fig. 9. Significant values (*p*-value ≤ 0.05) are marked in bold. "n/a" stands for not applicable.

Sample	Position*	*n*	Mean (μm)	σ	Min (μm)	Max (μm)	Difference between means (μm) and (*p*–values)	Difference between means (μm) and (*p*–values)	Difference between means (μm) and (*p*–values)
							No. 9006 vs. no. 8005 for the same zone	Z1 vs. Z2, Z2 vs. Z3 for the same vertical position in the same specimen	Z1vs. Z2, Z2 vs. Z3 for the same transverse position in the same specimen
No. 9006	Z1–1	26	4.43	1.06	2.86	6.74	0.23 (0.402)		
No. 8005	Z1–1	49	4.66	1.13	1.89	7.37		No. 9006 Z1–1 vs. Z2–1 **0.60 (0.013)**	
No. 9006	Z2–1	53	3.83	0.66	2.76	5.30	0.12 (0.419)	No. 9006 Z2–1 vs. Z3–1 0.07 (0.650)	
No. 8005	Z2–1	65	3.95	1.03	2.06	6.46			
No. 9006	Z3–1	38	3.76	0.80	2.32	5.55	0.32 (0.134)	No. 8005 Z1–1 vs. Z2–1 **0.71 (0.001)**	No. 9006 Z1 vs. Z2 **0.48 (0.011)**
No. 8005	Z3–1	44	4.08	1.05	2.22	7.53		No. 8005 Z2–1 vs. Z3–1 0.13 (0.554)	No. 9006 Z2 vs. Z3 0.14 (0.323)
No. 9006	Z1–2	26	4.71	1.27	2.76	8.38	**0.74 (0.024)**		No. 8005 Z1 vs. Z2 **0.59 (< 0.001)**
No. 8005	Z1–2	46	5.45	1.29	2.94	10.43		No. 9006 Z1–2 vs. Z2–2 0.33 (0.200)	No. 8005 Z2 vs. Z3 0.09 (0.595)
No. 9006	Z2–2	48	4.38	0.90	2.87	7.00	**0.62 (0.001)**	No. 9006 Z2–2 vs. Z3–2 0.30 (0.144)	
No. 8005	Z2–2	59	5.00	0.97	2.94	7.16		No. 8005 Z1–2 vs. Z2–2 **0.45 (0.048)**	
No. 9006	Z3–2	40	4.68	1.01	2.57	7.76	0.40 (0.087)	No. 8005 Z2–2 vs. Z3–2 0.08 (0.720)	
No. 8005	Z3–2	38	5.08	1.00	3.02	7.78			
No. 9006	Z4–1	23	3.79	0.71	2.72	4.99	**0.72 (0.003)**		
No. 8005	Z4–1	58	4.51	1.02	2.15	7.11		No. 9006 Z4–1 vs. Z5–1 0.11 (0.594)	
No. 9006	Z5–1	24	3.68	0.72	2.54	5.19	n/a		No. 9006 Z4 vs. Z5 0.09 (0.615)
No. 9006	Z4–2	33	4.61	0.89	3.15	6.55	0.24 (0.272)		
No. 8005	Z4–2	52	4.85	1.01	3.07	6.90		No. 9006 Z4–2 vs. Z5–2 0.06 (0.811)	
No. 9006	Z5–2	24	4.67	1.08	2.79	7.48	n/a		
							No. 63 vs. no. 43 vs. no. 158/223 for the same zone	Z1 vs. Z2 for the same vertical position in the same specimen	Z1 vs. Z2 for the same transverse position in the same specimen
No. 63	Z1–1	36	3.37	0.59	2.39	4.97	No. 63 vs. no. 158/223 **0.40 (0.013)**		
No. 43	Z1–1	70	3.73	0.98	1.63	6.94	No. 43 vs. no. 158/223 **0.76 (< 0.001)**	No. 63 Z1–1 vs. Z2–1 **0.72 (< 0.001)**	
No. 158/223	Z1–1	29	2.97	0.66	2.03	4.52		No. 43 Z1–1 vs. Z2–1 0.26 (0.109)	
No. 63	Z2–1	24	4.09	0.75	2.84	5.85	No. 63 vs. no. 158/223 0.17 (0.404)	No. 158/223 Z1–1 vs. Z2–1 **0.95 (< 0.001)**	
No. 43	Z2–1	61	3.99	0.82	1.95	5.88	No. 43 vs. no. 158/223 0.07 (0.691)		
No. 158/223	Z2–1	56	3.92	0.83	2.17	6.14			No. 63 Z1 vs. Z2 **0.80 (< 0.001)**
No. 63	Z1–2	35	4.02	0.87	2.56	6.19	No. 63 vs. no. 158/223 **0.73 (0.001)**		No. 43 Z1 vs. Z2 **0.40 (0.001)**
No. 43	Z1–2	71	4.04	0.87	2.16	7.24	No. 43 vs. no. 158/223 **0.75 (< 0.001)**		No. 158/223 Z1 vs. Z2 **1.2 (< 0.001)**
No. 158/223	Z1–2	25	3.29	0.67	2.04	4.73		No. 63 Z1–2 vs. Z2–2 **0.95 (< 0.001)**	
No. 63	Z2–2	20	4.97	0.95	3.64	7.19		No. 43 Z1–2 vs. Z2–2 **0.58 (0.001)**	
No. 43	Z2–2	56	4.62	1.10	2.68	7.67	No. 63 vs. no. 158/223 0.28 (0.234)	No. 158/223 Z1–2 vs. Z2–2 **1.4 (< 0.001)**	
No. 158/223	Z2–2	55	4.69	0.85	3.02	7.09	No. 43 vs. no. 158/223 0.07 (0.688)		

4 Discussion

4.1 Microstructure and organic component relationship

Before discussing whether and how acidification may affect the microstructure of the brachiopod shell, it is important to examine the relationship between the microstructure and the number of organic components within the shell. It has already been stated that, in fossil and recent brachiopods, different shell microstructures have different numbers of shell organic components (Garbelli et al., 2014; Garbelli, 2017; Casella et al., 2018; Ye et al., 2018a).

This holds true for most rhynchonelliformean brachiopods: the primary layer of *M. venosa* consists of acicular and granular calcite (Williams, 1968, 1973, 1997; MacKinnon and Williams, 1974; Williams and Cusack, 2007; Casella et al., 2018). Analyses of electron backscatter diffraction show that the primary layer is a thin nanocrystalline layer with higher micro-hardness and smaller-sized calcite crystallites compared to those of the secondary layer (Griesshaber et al., 2004). In addition, each spherical and small unit is coated by a mixture of organics and amorphous calcium carbonate (Cusack et al., 2010). This, *per se*, may suggest a higher amount of organic components associated with the primary layer in contrast to other shell layers (i.e. secondary or in some species tertiary layer), but it has never been proven.

In fossils, the primary layer is likely absent or, if present, diagenetically altered, and it will luminesce (Grossman et al., 1991), suggesting that higher amounts of organics may be present. However, this has also been ascribed to the incorporation of magnesium into the lattice (Popov et al., 2007; Cusack et al., 2008). A report of higher sulfur concentration in the primary layer of the brachiopod *Terebratulina retusa* may suggest the presence of a sulfur-rich organic component, but backscatter electron imaging revealed contradictory results (England et al., 2007). Cusack et al. (2008) showed that, in the same species, the sulfate concentration is higher in the primary layer than in the secondary layer.

Since there is no conclusive evidence for this observation, we cannot relate the increase in thickness of the primary layer to changes in organics within the shell. With respect to previous findings (Williams, 1966; Parkinson et al., 2005), our results show that the thickness of the primary layer of *M. venosa* is much less uniform and shows an increase with growth, which is more evident *during-culturing* under low-pH conditions. However, disturbances (stress condition with handling before and at the start of the culturing) may also cause an abrupt change in thickness.

Endopunctae, which during life are filled with mantle expansions, are widely distributed in the shell of *M. venosa* and show the superficial hexagonal close-packing pattern documented by Cowen (1966). The biological function of endopunctae is still controversial, with some suggesting that, generally in living organisms, they serve as support and protection structures (Williams, 1956, 1997), as sensors, or as storage and respiration features (Pérez-Huerta et al., 2009). With more endopunctae filled by mantle expansions, the amount of organic tissue would increase in the same volume of shell. The density of endopunctae has been related to temperature, as species living at higher temperatures have greater endopunctae density (Campbell, 1965; Foster, 1974; Peck et al., 1987; Ackerly et al., 1993). The present analyses support the concept that the increase in endopunctae density may be related in part to ontogeny and to low-pH conditions. This may be expected, as organisms living under low-pH conditions have to up-regulate their internal pH to be able to calcify, as demonstrated in *M. venosa* by Jurikova et al. (2019) and also observed in other calcifiers such as corals (McCulloch et al., 2012; Movilla et al., 2014). This would require a higher energy cost and a larger respiration/storage surface would satisfy this requirement.

In addition to the thickness of the primary layer and the density of the endopunctae, the size changes in the individual fibres within the fibrous secondary layer may also contribute to the variability in organic components. Most of the recent rhynchonelliformean brachiopods, and *M. venosa* in particular, possess a shell mainly made of a fibrous secondary layer (Williams, 1997; Parkinson et al., 2005; Williams and Cusack, 2007). Each fibre of this layer is secreted by the mantle and it is ensheathed by an organic membrane (e.g. Jope, 1965; Williams, 1968; MacKinnon, 1974; Williams and Cusack, 2007; Cusack et al., 2008; Casella et al., 2018). Thus, with a decrease in size but within the same shell volume the surface area increases and with it the number of organic components. Recently, the relationship between the size of fibres and shell organic components was discussed in detail (Garbelli, 2017; Garbelli et al., 2017; Ye et al., 2018a). The main conclusion is that the smaller the calcite fibres, the higher the organic component in the shell (cf. Fig. 11). Thus, smaller fibres and a greater endopunctae density may lead to higher organic content per shell volume (Fig. 11).

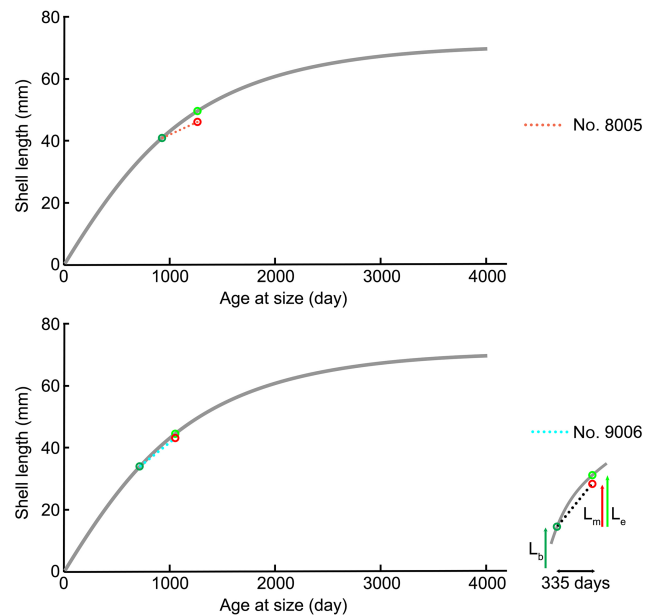### 4.2 Low pH and brachiopod microstructure

Several studies tried to understand how marine carbonate-shelled animals respond to ocean acidification, such as brachiopods (McClintock et al., 2009; Cross et al., 2015, 2016, 2018; Jurikova et al., 2019), bivalves (e.g. Berge et al., 2006; McClintock et al., 2009; Beniash et al., 2010; Parker et al., 2010; Melzner et al., 2011; Talmage and Gobler, 2011; Amaral et al., 2012; Hiebenthal et al., 2013; Coleman et al., 2014; Gobler et al., 2014; Milano et al., 2016), cold-water scleractinian corals (e.g. Form and Riebesell, 2011; McCulloch et al., 2012; Jantzen et al., 2013b; Büscher et al., 2017) and sea urchins (Suckling et al., 2015) (Table S1). The results of these studies show that, in general, seawater acidification reduces the growth rate of marine calcifiers (Michaelidis et al., 2005; Shirayama and Thornton, 2005; Berge et al., 2006; Bibby et al., 2007; Beniash et al., 2010; Nienhuis et al., 2010;
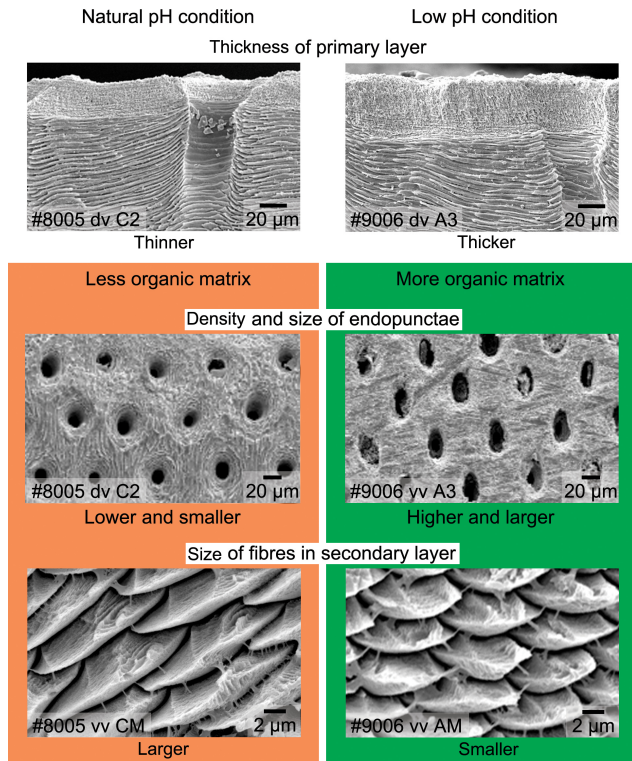
Figure 11. Relationship between the microstructure and the organic components of calcified shells of brachiopods. Position information: see Figs. 6 and 7; dv: dorsal valve; vv: ventral valve; CM: central middle part; AM: anterior middle part.

Figure 12. Projection of shell length of ventral valves on the von Bertalanffy growth function (grey line) $L_t = 71.53\ (1 - e^{-0.336(t-t^0)})$, source from Baumgarten et al. (2014); L_b: shell length at the beginning of culturing; L_m: measured shell growth at the end of culturing; Le: expected shell growth.

Thomsen and Melzner, 2010; Fernández-Reiriz et al., 2011; Melzner et al., 2011; Mingliang et al., 2011; Parker et al., 2011, 2012; Talmage and Gobler, 2011; Liu and He, 2012; Navarro et al., 2013; Milano et al., 2016).

For brachiopods, in the *Liothyrella uva* (Antarctic) and *Calloria inconspicua* (New Zealand), no ocean acidification effects on shell growth were detected by Cross et al. (2015, 2016, 2018), although the shells of the former species may rapidly dissolve in acidified waters (McClintock et al., 2009). However, *C. inconspicua* from the same locality in New Zealand (Paterson Inlet, Stewart Island) laid down a denser shell over the last 120 years, with nearby environmental conditions increasing by 0.6 °C from 1953 to 2016 and slightly increasing by 35.7 µatm in pCO$_2$ from 1998 to 2016 (Cross et al., 2018). These changes are in line with global trends of ocean pH and temperature since the industrial revolution (Caldeira and Wickett, 2005; Orr et al., 2005; IPCC, 2013). The present experiment showed that growth of specimens was not affected by the low-pH conditions; instead, their growth was similar to that of specimens cultured under control conditions (no. 9006, ~ 0.9 cm in the ventral valve, ~ 0.8 cm in the dorsal valve; no. 8005, ~ 0.5 cm in the ventral valve, ~ 0.4 cm in the dorsal valve). Based on the von Bertalanffy growth function, Baumgarten et al. (2014) calcu-

lated an expected growth increment and rate, and we compared those parameters with the measured ones under control and low-pH conditions. The results in Fig. 12 demonstrate that the measured individual growth rates are within the range of the ones of naturally growing individuals.

A limiting factor is the small database, but in general, the present observations agree with studies that show no or little impact of acidification on the growth rates of marine calcifiers (cf. Marchant et al., 2010; Thomsen et al., 2010; Range et al., 2011, 2012; Talmage and Gobler, 2011; Dickinson et al., 2012; Fernández-Reiriz et al., 2012; Liu and He, 2012; Hiebenthal et al., 2013; Cross et al., 2015, 2016, 2018), or even an increase in respiration, shell growth or metabolic rates after having experienced low-pH conditions (Wood et al., 2008; Cummings et al., 2011; Parker et al., 2012). We note however that a combined effect of multiple stressors, such as low pH, lower dissolved oxygen and higher temperature or scarce food availability is more complex and potentially detrimental. For instance, Steckbauer et al. (2015) reported that hypoxia and increased pCO$_2$ could significantly reduce the respiration rate of some marine invertebrates (Anthozoa, Gastropoda, Echinoidea and Crustacea). On the other hand, the highest growth rate in the bivalve *Macoma balthica* (*Limecola balthica* (Linnaeus, 1758)) was observed in seawater with low O$_2$ and high pH (Jansson et al., 2015). Gobler et al. (2014) reported that juveniles of the bivalves *Argopecten irradians* (Lamarck, 1819) and *Mercenaria mercenaria* (Linnaeus, 1758) were not affected by hypoxia or

acidification being applied individually, but the growth rate decreased when juveniles were exposed to both conditions simultaneously.

To explore the effects of acidification on brachiopod biomineralization, the microstructures of the specimens cultured for 214 days (no. 43, pH $= 7.66 \pm 0.04$; and no. 63, pH $= 7.44 \pm 0.08$) and the other population cultured for 335 days (no. 8005, pH $= 8.0$ to 8.15 ± 0.05; and no. 9006, pH $= 7.6$ to 7.35 ± 0.05) were investigated in detail. No conclusive consideration can be carried out on the specimens cultured for 214 days (no. 43 and no. 63), but in the other culturing experiments conducted for 335 days, the microstructure produced by the specimen cultured under low-pH conditions was different from that produced under control conditions: (1) the thickness of the primary layer increased with culturing (Fig. S1a–d); (2) the density and size of the endopunctae were higher (Fig. 1e–h); and (3) the fibres of the secondary layer were smaller. The punctal pattern detected here is different from that observed by Cross et al. (2018), who recorded no change in the punctal density of the ventral valve of *C. inconspicua* on specimens from the last 120 years. Also different is the trend in size of the endopunctae, which measured in the dorsal valve by Cross et al. (2018) seems to decrease. However, the slight environmental changes in the natural environment (references in Cross et al., 2018) are very different from those of our culturing experiments. Furthermore, the size of the endopunctae was measured from the dorsal valve only by Cross et al. (2018), whereas the increase in size we report was observed only from the ventral valve of *M. venosa*. A potential factor controlling this could be the duration of culturing under low-pH conditions. We note, however, that during the second phase of this acidification experiment (pH $= 7.35$), the seawater was strongly undersaturated with respect to calcite ($\Omega_{\mathrm{cal}} = 0.6$), suggesting that the observed structural changes could also be linked to the saturation state. Conversely, the duration of low-pH conditions as a controlling factor is also in line with the few data available in the literature on microstructural changes during acidification. Milano et al. (2016) reported no significant difference in the prismatic microstructure of the cockle *Cerastoderma edule* when cultured under low-pH conditions for about 2 months, except for dissolution of ontogenetically younger parts of the shell. Similarly, a study by Stemmer et al. (2013) on the clam *Arctica islandica* revealed that there was no effect on the shape and size of the crystals in the homogeneous microstructure after 3 months of culturing at low pH (Table S1). However, the experiments conducted by Fitzer et al. (2014a, b) for 6 months on the blue mussel *Mytilus edulis* showed that the animals exposed to low pH and high $p\mathrm{CO}_2$ tend to produce less organized, disorientated calcite crystals and an unordered layer structure.

Thus, in bivalves, and similar to our observations, the duration of culturing may be crucial in recording significant effects. The present results lend support to the microstructure variation observed in brachiopods during the end-Permian extinction event and concomitant ocean acidification (Garbelli et al., 2017). During this event, both Strophomenata and Rhynchonellata produced more organic-rich shells to cope with the long-term and protracted seawater acidification effects (Garbelli et al., 2017).

4.3 Stable isotope variation under low-pH conditions

Brachiopod shells are commonly used as archives for deep-time paleoenvironmental reconstructions as they potentially record the original geochemical composition of the seawater they lived in (Grossman et al., 1993; Banner and Kaufman, 1994; Mii and Grossman, 1994; Mii et al., 2001; Brand et al., 2003, 2011, 2016; Jurikova et al., 2019). Several studies suggest that carbon and oxygen isotope compositions of the secondary layer of brachiopod shells, especially slow-growing species – and particularly the innermost shell parts – tend to be close to equilibrium with the ambient seawater temperature (e.g. Popp et al., 1986; Carpenter and Lohmann, 1995; Parkinson et al., 2005; Brand et al., 2013, 2015, 2016; Takayanagi et al., 2013; Yamamoto et al., 2013). Recently, Bajnai et al. (2018) documented that brachiopods do not incorporate oxygen isotopes in thermodynamic equilibrium with ambient seawater, and appear to be subjected to taxon-specific growth-rate-induced kinetic effects. The documented isotopic offset appears to be relatively constant throughout the range of brachiopod shell production from cold to warm environments. Thus, the brachiopod oxygen isotope composition, when corrected for the seawater-^{18}O contribution, records ambient water temperatures close to those observed for their ambient environment (Brand et al., 2013). Overall, the δ^{18}O values of brachiopods remain a mainstay and robust proxies of paleoenvironmental temperature conditions.

In general, the measured δ^{13}C (between $-8.05\,‰$ and $+0.45\,‰$) and δ^{18}O (between $-3.04\,‰$ and $+0.21\,‰$) values of the secondary layer produced during growth in the natural environment (Fig. 10) are similar to previous results from the shells of *M. venosa* (Penman et al., 2013; Ullmann et al., 2017; Romanin et al., 2018). Furthermore, the present results show that there are no significant differences in δ^{13}C and δ^{18}O values between the dorsal and ventral valves (*p*-values in δ^{13}C and δ^{18}O of no. 8005 are 0.437 and 0.491, respectively, and *p*-values in δ^{13}C and δ^{18}O of no. 9006 are 0.862 and 0.910, respectively), which is in agreement with previous findings (e.g. Parkinson et al., 2005; Brand et al., 2015; Romanin et al., 2018).

In the naturally grown shell *before-culturing*, the δ^{13}C and δ^{18}O values are relatively stable along the ontogenetic direction (Table S2), except for the depleted values at approximately mid-shell length in both no. 8005 and no. 9006. In particular, in no. 9006, in this part of the shell values drop to about $-6\,‰$ for δ^{13}C and $-2\,‰$ for δ^{18}O values (Fig. 10). Since the samples were taken from the mid-shell layer and not from the shell interior, we can exclude the isotope nega-

tive shift being produced by shell material added during the *during-culturing* shell thickening. While this drop may be an artefact of both sampling and analytical uncertainties, a possibility also exists that it could be linked to shell repair processes. Brachiopods are well known to show a remarkable shell repair ability (Cross et al. 2015, 2016), and thus it cannot be ruled out that this shell part, although originally formed early in life under natural conditions, also contains a contribution from material precipitated in the culture seawater later in life, in particular under low-pH conditions. Also, negative isotope excursions of a similar magnitude were recorded in *M. venosa* specimens from the South America shelf by Ullmann et al. (2017) and Romanin et al. (2018). Ullmann et al. (2017) implied that these variable $\delta^{13}C$ and $\delta^{18}O$ values indicate isotope disequilibrium with ambient waters in Terebratellids. In contrast, Romanin et al. (2018), who also analysed specimens collected from Comau Fjord, attributed the negative isotope excursion to environmental perturbations, in particular, to changes in seawater productivity and temperature, and/or to anthropogenic activities. Negative shifts in both $\delta^{13}C$ and $\delta^{18}O$ values during ontogeny have also been observed in the brachiopod *Terebratella dorsata*, which co-occurs with *M. venosa* and which has been explained by the effect of resorption in corresponding muscle scar areas (Carpenter and Lohmann, 1995). Here, we follow the interpretation of Romanin et al. (2018) to explain the mid-shell excursion observed in our specimens.

The most prominent change in $\delta^{13}C$ values was observed in the secondary layer produced *during-culturing* under low-pH conditions ($\delta_{13}C$ VPDB: $\sim -25\,‰$), reflecting the composition of the $\delta^{13}C_{DIC}$ ($\delta^{13}C$ VPDB: $-24\,‰$ for the low-pH/high-pCO$_2$ conditions). The $\delta^{13}C$ values were significantly depleted by more than $20\,‰$ in the specimens cultured under low-pH/high-pCO$_2$ conditions (pH 7.60 and pH 7.35; no. 9004, no. 9005 and no. 9006) (Fig. 10, Appendix A, Table S2), whereas the depletion was lower and only a few per mil (about $0.9\,‰$–$1.2\,‰$) in the control specimens (pH 8.00 and 8.15; no. 8004 and no. 8005). This demonstrates that the $\delta^{13}C$ values of *M. venosa* to a large extent reflect the composition of the CO_2 source and thus present a valuable geochemical archive. Similar observations have also been reported for other calcifiers cultured under controlled experimental settings with pH mediated by CO_2-bubbling. For a comparison, Hahn et al. (2014) reported a decreasing trend of about $10\,‰$ in $\delta^{13}C$ values in the blue mussel *Mytilus edulis* when exposed to seawater conditions of pH 8.03 (pCO$_2$ 612 µatm) and pH 7.21 (pCO$_2$ 4237 µatm). In corals, a species-specific $\delta^{13}C$ response to high-pCO$_2$ conditions was reported by Krief et al. (2010) of more negative $2.3\,‰$ and $1.5\,‰$ $\delta^{13}C$ values in *Porites* sp. after 14 months of culturing under low-pH conditions (pH 7.49, pCO$_2$ 1908 µatm and 7.19 pCO$_2$, 3976 µatm), whereas no significant difference was found in other coral species, such as *Stylophora pistillata* (Esper, 1797).

In our culturing experiments, oxygen isotope compositions of the shells record only a minor depletion *during-culturing* under different pH conditions ($\delta^{18}O$ (VPDB): $-6.4\,‰$ to $-7.9\,‰$/(VSMOW): $\sim +23.6\,‰$ to $+24.3\,‰$) in comparison to the values observed in the shell parts grown under natural conditions, following the changes in $\delta^{18}O_{H_2O}$.

The fractionation of carbon and oxygen isotopes between phases – brachiopod calcite and culture seawater – is defined as $\Delta^{13}C_{cal\text{-}DIC}$ or $\Delta^{18}O_{cal\text{-}sw} = 1000 \times \ln\alpha_{cal\text{-}DIC/sw}$, where $\alpha_{cal\text{-}DIC/sw} = [^{13}C/^{12}C]_{cal}/[^{13}C/^{12}C]_{DIC}$ or $[^{18}O/^{16}O]_{cal}/[^{18}O/^{16}O]_{sw}$, respectively. The calculated values based on our culture measurements are presented in Table 11.

For carbon isotopes, we observe variable $\Delta^{13}C_{cal\text{-}DIC}$ between the different specimens and culturing treatments, and it is inconclusive whether this is linked to culturing conditions, differences between individuals or an ontogenetic component. It appears that there is about a $2\,‰$ difference between the control specimen and samples from the acidification treatments (pH 7.35), with the last one being, strikingly, closer to the equilibrium with seawater DIC. Possibly, this illustrates the variability in kinetic effects (Bajnai et al., 2018), but may also be linked to changes in the source $\delta^{13}C_{DIC}$ in the control treatment. More studies are needed to fully answer this question.

Similarly, for oxygen isotopes, we find variable $\Delta^{18}O_{cal\text{-}sw}$ with an apparent trend with pH. These values are offset from the equilibrium $\Delta^{18}O_{cal\text{-}sw}$ ($\Delta^{18}O_{cal\text{-}sw} = 32.9$ at 10°C) determined by Watkins et al. (2013, 2014). This suggests that *M. venosa* present non-equilibrium growth-rate-related isotope effects up to about $-2.9\,‰$, larger than the approx. $-1.5\,‰$ previously recorded by Bajnai et al. (2018). Provided that this offset can be constrained, brachiopods continue to present robust archives for palaeo-temperature reconstructions.

In summary, although it appears that variable growth rates present the most prominent confounding parameter complicating the interpretation of carbon and oxygen data, provided that we account for them, our results support the notion that brachiopods present robust geochemical archives, even when stressed by ocean acidification.

5   Conclusions

This study combines the analysis of shell microstructures on six specimens consisting of 1932 fibre size measurements, 170 primary layer thickness measurements, 256 punctal density and diameter measurements and stable isotope geochemistry on five specimens of 79 sample analyses, on brachiopods cultured under low-pH conditions for different time intervals. The results suggest the following conclusions.

In brachiopod specimens cultured for a period of 11 months, the microstructure produced by the specimen cultured at low pH (from pH 7.60 to pH 7.35) is different from

Table 11. Calculated carbon and oxygen fractionation factors for brachiopods based on cultured *M. venosa* and culture seawater.

Sample	Treatment ID	Avg. $\Delta^{13}C_{cal\text{-}DIC}$	Avg. $\Delta^{18}O_{cal\text{-}sw}$	Growth temperature
No. 8004	Control	−4.06	29.99	10 °C
No. 9005	Acidification pH 7.35	−1.21	30.92	10 °C
No. 9004	Acidification pH 7.35	−2.23	30.70	10 °C

that produced under control conditions (pH 8.00 and 8.15). In particular, the microstructure of shells produced at low pH tends to be more organic-rich, a result that lends strong support to brachiopod microstructure variations observed in fossil counterparts and the related effect of ocean acidification.

Brachiopod shell parts precipitated during culturing conditions of low pH for about 1 year record a change in the microstructure but not in the growth rate.

Their $\delta^{13}C$ and $\delta^{18}O$ values are rather constant during growth but experience a sharp drop *during-culturing*. In particular, the $\delta^{13}C$ values dropped abruptly in specimens cultured for 1 year under low-pH conditions. This drop is related to the source of carbon dioxide gas used in the culture set-up.

Brachiopods are thus faithful recorders of the ambient carbon and oxygen isotope compositions, even when stressed by environmental perturbations such as ocean acidification.

The present observations are invaluable in using proxies and shell morphologic features for studying ocean acidification events and changes in atmospheric CO_2 contents in the geologic past.

Data availability. All data pertinent to this paper and its reported findings can be found in the paper itself or in the associated Supplement.

Appendix A

Table A1. Carbon and oxygen isotope compositions of cultured brachiopod shell sampled in the secondary layer, along the growth increments from margin to umbo (shown in the paper Fig. 10).

Valve	No. isotope test	Position (Milan)	Position (GEOMAR)	$\delta^{13}C$ (‰ V-PDB)	$\sigma\delta^{13}C$ (‰ V-PDB)	$\delta^{18}O$ (‰ V-PDB)	$\sigma\delta^{18}O$ (‰ V-PDB)
dorsal valve	8005-e	edge–600 ppm CO_2		−1.42	0.04	−5.53	0.03
dorsal valve	8005-1	Chile; b-1		−1.54	0.04	−2.68	0.07
dorsal valve	8005-2	b-2		−0.29	0.05	−0.19	0.04
dorsal valve	8005-3	b-3		0.09	0.04	−0.05	0.06
dorsal valve	8005-4	b-4		−0.19	0.06	−0.15	0.04
dorsal valve	8005-5	b-5		−0.29	0.05	−0.11	0.05
dorsal valve	8005-6	b-6		−0.14	0.04	−0.27	0.06
dorsal valve	8005-7	b-7		−0.54	0.03	−0.27	0.04
dorsal valve	8005-8	b-8		−0.73	0.04	−0.22	0.04
dorsal valve	8005-9	b-9		0.25	0.03	0.21	0.07
dorsal valve	8005-10	b-10 umbo area		0.33	0.03	−0.56	0.04
ventral valve	8005-e1	p edge-1–600 ppm CO_2		−1.34	0.04	−5.70	0.04
ventral valve	8005-e2	p edge-2–600 ppm CO_2		−1.82	0.03	−5.85	0.04
ventral valve	8005-1x	p-1		−0.91	0.06	−1.46	0.04
ventral valve	8005-2x	p-2		−0.84	0.03	−0.54	0.04
ventral valve	8005-3x	p-3		−0.92	0.06	−0.49	0.05
ventral valve	8005-4x	p-4		−0.78	0.05	−0.92	0.05
ventral valve	8005-5x	p-5		−2.02	0.02	−0.83	0.05
ventral valve	8005-6x	p-6		−0.48	0.05	−0.36	0.04
ventral valve	8005-7x	p-7		0.16	0.02	0.14	0.04
ventral valve	8005-8x	p-8		0.32	0.05	0.08	0.03
ventral valve	8005-9x	p-9		0.45	0.04	−0.62	0.03
ventral valve	8005-10x	p-10 umbo area		0.36	0.05	−0.87	0.05
dorsal valve	9006D-e1	b edge 1–4000 ppm CO_2		−21.82	0.02	−5.33	0.03
dorsal valve	9006D-e2	be-2–2000 ppm CO_2		−19.69	0.06	−5.29	0.05
dorsal valve	9006D-e3	be-3–2000 ppm CO_2		−19.30	0.05	−5.50	0.02
dorsal valve	9006D-e4	be-4–2000 ppm CO_2		−17.05	0.04	−5.63	0.04
dorsal valve	9006D-eT	bTransition		−8.13	0.05	−4.25	0.04
dorsal valve	9006D-1	b-1		−2.94	0.06	−2.16	0.04
dorsal valve	9006D-2	b-2		−1.30	0.05	−0.56	0.03
dorsal valve	9006D-3	b-3		−0.53	0.03	−0.19	0.04
dorsal valve	9006D-4	b-4		−1.41	0.02	−0.44	0.04
dorsal valve	9006D-5	b-5		−3.65	0.04	−1.18	0.06
dorsal valve	9006D-6	b-6		−0.87	0.04	−0.04	0.05
dorsal valve	9006D-7	b-7		−1.19	0.06	−0.05	0.05
dorsal valve	9006D-8	b-8 umbo area		−1.16	0.03	0.05	0.04
ventral valve	9006v-e1	p edge-1–4000 ppm CO_2		−20.84	0.04	−5.32	0.03
ventral valve	9006v-e2	pe-2–2000 ppm CO_2		−20.86	0.05	−5.74	0.03
ventral valve	9006v-e3	pe-3–2000 ppm CO_2		−19.98	0.04	−6.09	0.05
ventral valve	9006v-e4	pe-4–2000 ppm CO_2		−20.15	0.07	−6.33	0.04
ventral valve	9006v-eT	p transition		−10.21	0.04	−5.32	0.04
ventral valve	9006v-1	p-1		−2.18	0.03	−2.00	0.02
ventral valve	9006v-2	p-2		−1.68	0.05	−1.15	0.05
ventral valve	9006v-3	p-3		−2.99	0.04	−1.48	0.02
ventral valve	9006v-4	p-4		−1.36	0.04	−0.83	0.03
ventral valve	9006v-5	p-5		−8.05	0.05	−2.89	0.04
ventral valve	9006v-6	p-6		−1.62	0.03	-0.35	0.03
ventral valve	9006v-7	p-7		−2.58	0.04	−0.57	0.02
ventral valve	9006v-8	p-8		−3.13	0.03	−0.69	0.03
ventral valve	9006v-9	p-9		−1.53	0.04	−0.12	0.05
ventral valve	9006v-10	p-10		−1.67	0.04	−0.03	0.04
ventral valve	9006v-11	p-11		−2.58	0.03	−0.19	0.03
ventral valve	9006v-12	p-12		−2.93	0.04	−0.43	0.04
ventral valve	9006v-13	p-13 umbo area		−3.56	0.04	−1.00	0.04
ventral valve	9004-1		Low pH: 4000 ppm	−27.09	0.03	−6.97	0.08
ventral valve	9004-2		Low pH: 4000 ppm	−24.53	0.13	−6.18	0.14
ventral valve	9004-3 (4000 ppm border)		Low pH: 4000 ppm	−23.47	0.05	−6.04	0.11

Table A1. Continued.

Valve	No. isotope test	Position (Milan)	Position (GEOMAR)	δ^{13}C (‰ V-PDB)	$\sigma\delta^{13}$C (‰ V-PDB)	δ^{18}O (‰ V-PDB)	$\sigma\delta^{18}$O (‰ V-PDB)
ventral valve	9004-4		Low pH: 2000 ppm	−22.31	0.07	−6.23	0.05
ventral valve	9004-5		Low pH: 2000 ppm	−23.37	0.03	−6.10	0.06
ventral valve	9004-6		Low pH: 2000 ppm	−23.84	0.02	−6.62	0.05
ventral valve	9004-7		Low pH: 2000 ppm	−25.04	0.04	−6.91	0.06
ventral valve	9004-16		Low pH: 2000 ppm	−21.50	0.02	−6.57	0.05
ventral valve	9004-17		Low pH: 2000 ppm	−21.46	0.02	−6.57	0.06
ventral valve	9004-18		Low pH: 2000 ppm	−13.70	0.07	−6.57	0.08
ventral valve	9004-19		Low pH: 2000 ppm	−11.95	0.03	−5.37	0.03
ventral valve	9004-20		Low pH: 2000 ppm	−9.69	0.04	−5.56	0.08
ventral valve	9004-21 (nat. border)		Nature	−7.34	0.02	−4.92	0.03
ventral valve	9004-29		Nature	−9.24	0.03	−3.04	0.04
ventral valve	9004-umbo		Nature	−1.12	0.08	−0.55	0.05
ventral valve	9005-1		Low pH: 4000 ppm	−25.91	0.07	−6.56	0.11
ventral valve	9005-2		Low pH: 4000 ppm	−23.72	0.03	−6.15	0.07
ventral valve	9005-3 (4000 ppm border)		Low pH: 4000 ppm	−22.15	0.04	−6.00	0.07
ventral valve	9005-4 (equal to 19)		Low pH: 2000 ppm	−12.67	0.05	−5.20	0.05
ventral valve	9005-umbo		Nature	−3.91	0.03	−1.67	0.05
ventral valve	8004-1		Control (to 4000 ppm)	−6.80	0.04	−7.39	0.07
ventral valve	8004-2		Control (to 4000 ppm)	−5.35	0.03	−6.79	0.04
ventral valve	8004-3 (4000 ppm borderr)		Control (to 4000 ppm)	−4.59	0.04	−6.32	0.04
ventral valve	8004-4 (equal to 19)		Control (to 2000 ppm)	−3.53	0.04	−5.37	0.03
ventral valve	8004-umbo		Nature	−0.89	0.04	−2.39	0.06

Appendix B

Table B1. Carbon and oxygen isotope composition of artificial seawater from culture experiments at GEOMAR, Kiel, measured in July 2017. C2 refers to the control treatments and C3 represents the acidification treatment. The standard deviation (σ) is based on three repeated measurements of each sample.

Aquarium ID	δ^{13}C (‰ V-PDB)	$\sigma\delta^{13}$C (‰ V-PDB)	δ^{18}O (‰ VSMOW)	$\sigma\delta^{18}$O (‰ VSMOW)
C2 (control)	−2.03	0.029	−6.685	0.03
C3 (low pH)	−23.633	0.02	−6.88	0.012

Author contributions. FY, LA and HJ designed the study and wrote the manuscript. FY prepared the specimens and carried out the microstructure analyses. HJ, UB, GC, and DŠ made the stable isotope measurements and/or helped with the interpretation of the data. HJ, DH and CH carried out the culturing experiments at GEOMAR, Kiel, and JL at AWI, Bremerhaven. JL provided *M. venosa* individuals from nature.

References

Ackerly, S., Cisne, J. L., Railsback, L. B., and Anderson, T. F.: Punctal density in the Ordovician orthide brachiopod *Paucicrura rogata*: anatomical and paleoenvironmental variation, Lethaia, 26, 17–24, https://doi.org/10.1111/j.1502-3931.1993.tb01506.x, 1993.

Amaral, V., Cabral, H. N., and Bishop, M. J.: Moderate acidification affects growth but not survival of 6–month–old oysters, Aquat. Ecol., 46, 119–127, https://doi.org/10.1007/s10452-011-9385-5, 2012.

Atkinson, M. J. and Bingman, C.: Elemental composition of commercial seasalts, J. Aquaricult. Aquat. Sci., 8, 39–43, 1998.

Bajnai, D., Fiebig, J., Tomašových, A., Milner, G. S., Rollin-Bard, C., Raddztz, J., Löffler, N., Primo-Romos, C., and Brand, U.: Assessing kinetic fractionation in brachiopod calcite using clumped isotopes, Sci. Rep., 8, 533, https://doi.org/10.1038/s41598-017-17353-7, 2018.

Banner, J. L. and Kaufman, J.: The isotopic record of ocean chemistry and diagenesis preserved in non-luminescent brachiopods from Mississippian carbonate rocks, Illinois and Missouri, Geol. Soc. Am. Bull., 106, 1074–1082, https://doi.org/10.1130/0016-7606(1994)106<1074:TIROOC>2.3.CO;2, 1994.

Baumgarten, S., Laudien, J., Jantzen, C., Häussermann, V., and Försterra, G.: Population structure, growth and production of a recent brachiopod from the Chilean fjord region, Mar. Ecol., 35, 401–413, https://doi.org/10.1111/maec.12097, 2014.

Beniash, E., Ivanina, A., Lieb, N. S., Kurochkin, I., and Sokolova, I.: Elevated level of carbon dioxide affects metabolism and shell formation in oysters *Crassostrea virginica*, Mar. Ecol., 419, 95–108, https://doi.org/10.3354/meps08841, 2010.

Berge, J. A., Bjerkeng, B., Pettersen, O., Schaanning, M. T., and Øxnevad, S.: Effects of increased sea water concentrations of CO_2 on growth of the bivalve *Mytilus edulis* L, Chemosphere, 62, 681–687, https://doi.org/10.1016/j.chemosphere.2005.04.111, 2006.

Bibby, R., Cleall-Harding, P., Rundle, S., Widdicombe, S., and Spicer, J.: Ocean acidification disrupts induced defences in the intertidal gastropod *Littorina littorea*, Biol. Lett., 3, 699–701, https://doi.org/10.1098/rsbl.2007.0457, 2007.

Brand, U. and Veizer, J.: Chemical diagenesis of a multi-component carbonate system-1. Trace elements, J. Sediment. Petrol., 50, 1219–1236, https://doi.org/10.1306/212f7bb7-2b24-11d7-8648000102c1865d, 1980.

Brand, U., Logan, A., Hiller, N., and Richardson, J.: Geochemistry of modern brachiopods: applications and implications for oceanography and paleoceanography, Chem. Geol., 198, 305–334, https://doi.org/10.1016/s0009-2541(03)00032-9, 2003.

Brand, U., Logan, A., Bitner, M. A., Griesshaber, E., Azmy, K., and Buhl, D.: What is the ideal proxy of Palaeozoic seawater chemistry?, Mem. Assoc. Australas., 41, 9–24, 2011.

Brand, U., Azmy, K., Bitner, M. A., Logan, A., Zuschin, M., Came, R., and Ruggiero, E.: Oxygen isotopes and $MgCO_3$ in brachiopod calcite and a new paleotemperature equation, Chem. Geol., 359, 23–31, https://doi.org/10.1016/j.chemgeo.2013.09.014, 2013.

Brand, U., Azmy, K., Griesshaber, E., Bitner, M. A., Logan, A., Zuschin, M., Ruggiero, E., and Colin, P. L.: Carbon isotope composition in modern brachiopod calcite: A case of equilibrium with seawater?, Chem. Geol., 411, 81–96, https://doi.org/10.1016/j.chemgeo.2015.06.021, 2015.

Brand, U., Blamey, N., Garbelli, C., Griesshaber, E., Posenato, R., Angiolini, L., Azmy, K., Farabegoli, E., and Came, R.: Methane Hydrate: Killer cause of Earth's greatest mass extinction, Palaeoworld, 25, 496–507, https://doi.org/10.1016/j.palwor.2016.06.002, 2016.

Büscher, J. V., Form, A. U., and Riebesell, U.: Interactive effects of ocean acidification and warming on growth, fitness and survival of the cold–water coral *Lophelia pertusa* under different food availabilities, Front. Mar. Sci., 4, 101, https://doi.org/10.3389/fmars.2017.00101, 2017.

Caldeira, K. and Wickett, M. E.: Anthropogenic carbon and ocean pH, Nature, 425, 365, https://doi.org/10.1038/425365a, 2003.

Caldeira, K. and Wickett, M. E.: Ocean model predictions of chemistry changes from carbon dioxide emissions to the atmosphere and ocean, J. Geophys. Res., 110, C09S04, https://doi.org/10.1029/2004jc002671, 2005.

Campbell, K. S. W.: Australian Permian terebratuloids, Bur. Min. Resour. Geol. Geophys. Aust. Bull., 68, l–113, 1965.

Carpenter, S. J. and Lohmann, K. C.: $\delta^{18}O$ and $\delta^{13}C$ values of modern brachiopod shells, Geochim. Cosmochim. Ac., 59, 3749–3764, https://doi.org/10.1016/0016-7037(95)00291-7, 1995.

Casella, L., Griesshaber, E., Simonet Roda, M., Ziegler, A., Mavromatis, V., Henkel, D., Laudien, J., Häussermann, V., Neuser, R.

D., Angiolini, L., Dietzel, M., Eisenhauer, A., Immenhauser, A., Brand, U., and Schmahl, W. W.: Micro- and nanostructures reflect the degree of diagenetic alteration in modern and fossil brachiopod shell calcite: a multi–analytical screening approach (CL, FE–SEM, AFM, EBSD), Palaeogeogr. Palaeocl., 502, 13–30, https://doi.org/10.1016/j.palaeo.2018.03.011, 2018.

Coleman, D. W., Byrne, M., and Davis, A. R.: Molluscs on acid: gastropod shell repair and strength in acidifying oceans, Mar. Ecol. Prog. Ser., 509, 203–211, https://doi.org/10.3354/meps10887, 2014.

Comeau, S., Gorsky, G., Jeffree, R., Teyssié, J.-L., and Gattuso, J.-P.: Impact of ocean acidification on a key Arctic pelagic mollusc (*Limacina helicina*), Biogeosciences, 6, 1877–1882, https://doi.org/10.5194/bg-6-1877-2009, 2009.

Cowen, R.: The distribution of punctae on the brachiopod shell, Geol. Mag., 103, 269–275, https://doi.org/10.1017/s0016756800052857, 1966.

Cross, E. L., Peck, L. S., and Harper, E. M.: Ocean acidification does not impact shell growth or repair of the Antarctic brachiopod *Liothyrella uva* (Broderip, 1833), J. Exp. Mar. Biol. Ecol., 462, 29–35, https://doi.org/10.1016/j.jembe.2014.10.013, 2015.

Cross, E. L., Peck, L. S., Lamare, M. D., and Harper, E. M.: No ocean acidification effects on shell growth and repair in the New Zealand brachiopod *Calloria inconspicua* (Sowerby, 1846), ICES J. Mar. Sci., 73, 920–926, https://doi.org/10.1093/icesjms/fsv031, 2016.

Cross, E. L., Harper, E. M., and Peck, L. S.: A 120-year record of resilience to environmental change in brachiopods, Glob. Chang. Biol., 24, 2262–2271, https://doi.org/10.1111/gcb.14085, 2018.

Cummings, V., Hewitt, J., Rooyen, A. V., Currie, K., Beard, S., Thrush, S., Norkko, J., Barr, N., Heath, P., Halliday, N. J., Sedcole, R., Gomez, A., McGraw, C., and Metcalf, V.: Ocean acidification at high latitudes: potential effects on functioning of the Antarctic bivalve *Laternula elliptica*, PLoS ONE, 6, e16069, https://doi.org/10.1371/journal.pone.0016069, 2011.

Cusack, M., Dauphin, Y., Cuif, J. P., Salomé, M., Freer, A., and Yin, H.: Micro–XANES mapping of sulphur and its association with magnesium and phosphorus in the shell of the brachiopod, *Terebratulina retusa*, Chem. Geol., 253, 172–179, https://doi.org/10.1016/j.chemgeo.2008.05.007, 2008.

Cusack, M., Chung, P., Dauphin, Y., and Pérez–Huerta, A.: Brachiopod primary layer crystallography and nanostructure, in: Alvarez, F., and Curry, G. B. (Eds.): Evolution and Development of the Brachiopod Shell, Special Papers in Palaeontology, 84, Aberystwyth, Palaeontological Association, 99–105, 2010.

Crippa, G., Angiolini, L., Bottini, C., Erba, E., Felletti, F., Frigerio, C., Hennissen, J. A. I., Leng, M. J., Petrizzo, M. R., Raffi, I., Raineri, G., and Stephenson, M. H.: Seasonality fluctuations recorded in fossil bivalves during the early Pleistocene: Implications for climate change, Palaeogeogr. Palaeocl., 446, 234–251, https://doi.org/10.1016/j.palaeo.2016.01.029, 2016a.

Crippa, G., Ye, F., Malinverno, C., and Rizzi, A.: Which is the best method to prepare invertebrate shells for SEM analysis? Testing different techniques on recent and fossil brachiopods, Boll. Soc. Paleontol. I., 55, 111–125, 2016b.

Dickinson, G. H., Ivanina, A. V., Matoo, O. B., Pörtner, H. O., Lannig, G., Bock, C., Beniash, E., and Sokolova, I. M.: Interactive effects of salinity and elevated CO_2 levels on juvenile Eastern oysters, *Crassostrea virginica*, J. Exp. Biol., 215, 29–43, https://doi.org/10.1242/jeb.061481, 2012.

England, J., Cusack, M., and Lee, M. R.: Magnesium and sulphur in the calcite shells of two brachiopods, *Terebratulina retusa* and *Novocrania anomala*, Lethaia, 40, 2–10, https://doi.org/10.1111/j.1502-3931.2006.00001.x, 2007.

Feely, R. A., Sabine, C. L., Lee, K., Berelson, W., Kleypas, J., Fabry, V. J., and Millero, F. J.: Impact of anthropogenic CO_2 on the $CaCO_3$ system in the oceans, Science, 305, 362–366, https://doi.org/10.1126/science.1097329, 2004.

Fernández-Reiriz, M. J., Range, P., Alvarez-Salgado, X. A., and Labarta, U.: Physiological energetics of juvenile clams *Ruditapes decussatus* in a high CO_2 coastal ocean, Mar. Ecol. Prog. Ser., 433, 97–105, https://doi.org/10.3354/meps09062, 2011.

Fernández-Reiriz, M. J., Range, P., Alvarez-Salgado, X. A., Espinosa, J., and Labarta, U.: Tolerance of juvenile *Mytilus galloprovincialis* to experimental seawater acidification, Mar. Ecol. Prog. Ser., 454, 65–74, https://doi.org/10.3354/meps09660, 2012.

Fitzer, S., Phoenix, V. R., Cusack, M., and Kamenos, N. A.: Ocean acidification impacts mussel control on biomineralisation, Sci. Rep., 4, 2045–2322, https://doi.org/10.1038/srep06218, 2014a.

Fitzer, S., Cusack, M., Phoenix, V. R., and Kamenos, N. A.: Ocean acidification reduces the crystallographic control in juvenile mussel shells, J. Struct. Biol., 188, 39–45, https://doi.org/10.1016/j.jsb.2014.08.007, 2014b.

Form, A. U. and Riebesell, U.: Acclimation to ocean acidification during long–term CO_2 exposure in the cold-water coral *Lophelia pertusa*, Glob. Change Biol., 18, 843–853, https://doi.org/10.1111/j.1365-2486.2011.02583.x, 2011.

Försterra, G., Häussermann, V., and Lueter, C.: Mass occurrence of the recent brachiopod *Magellania venosa* (Terebratellidae) in the fjords Comau and Renihue, northern Patagonia, Chile, Mar. Ecol., 29, 342–347, https://doi.org/10.1111/j.1439-0485.2008.00240.x, 2008.

Foster, M. W.: Recent Antarctic and Subantarctic brachiopods, Antarctic Research Series, 21, American Geophysical Union, Washington, D.C., 183 pp., https://doi.org/10.1029/ar021, 1974.

Garbelli, C.: Shell microstructures in Upper Permian brachiopods: implication for fabric evolution and calcification, Boll. Soc. Paleontol. I., 123, 541–560, 2017.

Garbelli, C., Angiolini, L., Brand, U., and Jadoul, F.: Brachiopod fabric, classes and biogeochemistry: Implications for the reconstruction and interpretation of seawater carbon–isotope curves and records, Chem. Geol., 371, 60–67, https://doi.org/10.1016/j.chemgeo.2014.01.022, 2014.

Garbelli, C., Angiolini, L., and Shen, S. Z.: Biomineralization and global change: A new perspective for understanding the end–Permian extinction, Geology, 45, 19–12, https://doi.org/10.1130/g38430.1, 2017.

Gobler, C. J., DePasquale, E. L., Griffith, A. W., and Baumann, H.: Hypoxia and acidification have additive and synergistic negative effects on the growth, survival, and metamorphosis of early life stage bivalves, PLoS ONE, 9, e83648, https://doi.org/10.1371/journal.pone.0083648, 2014.

Griesshaber, E., Schmahl, W., Neuser, R., Job, R., Bluem, M., and Brand, U.: Microstructure of brachiopod shells–An inorganic/organic fibre composite with nanocrystalline protec-

tive layer, Mater. Res. Soc. Symp. P., 844, Y9.3.1–Y9.3.6, https://doi.org/10.1557/proc-844-y9.3, 2004.

Grossman, E. L., Zhang, C., and Yancey, T. E.: Stable–isotope stratigraphy of brachiopods from Pennsylvanian shales in Texas, Geol. Soc. Am. Bull., 103, 953–965, https://doi.org/10.1130/0016-7606(1991)103<0953:sisobf>2.3.co;2, 1991.

Grossman, E. L., Mii, H., and Yancey, T. E.: Stable isotopes in Late Pennsylvanian brachiopods from the United Stated: Implications for Carboniferous paleoceanography, Geol. Soc. Am. Bull., 105, 1284–1296, https://doi.org/10.1130/0016-7606(1993)105<1284:siilpb>2.3.co;2, 1993.

Guinotte, J. M., Orr, J., Cairns, S., Freiwald, A., Morgan, L., and George, R.: Will human–induced changes in sea water chemistry alter the distribution of deep-sea scleractinian corals?, Front. Ecol. Environ., 1, 141–146, 2006.

Hahn, S., Rodolfo-Metalpa, R., Griesshaber, E., Schmahl, W. W., Buhl, D., Hall-Spencer, J. M., Baggini, C., Fehr, K. T., and Immenhauser, A.: Marine bivalve shell geochemistry and ultrastructure from modern low pH environments: environmental effect versus experimental bias, Biogeosciences, 9, 1897–1914, https://doi.org/10.5194/bg-9-1897-2012, 2012.

Hahn, S., Griesshaber, E., Schmahl, W. W., Neuser, R. D., Ritter, A., Hoffmann, R., Buhl, D., Niedermayr, A., Geske, A., and Immenhauser, A.: Exploring aberrant bivalve shell ultrastructure and geochemistry as proxies for past sea water acidification, Sedimentology, 61, 1625–1658, https://doi.org/10.1111/sed.12107, 2014.

Hiebenthal, C., Philipp, E. E. R., Eisenhauer, A., and Wahl, M.: Effects of seawater $p\mathrm{CO_2}$ and temperature on shell growth, shell stability, condition and cellular stress of Western Baltic Sea *Mytilus edulis* (L.) and *Arctica islandica* (L.), Mar. Biol., 160, 2073–2087, https://doi.org/10.1007/s00227-012-2080-9, 2013.

IPCC: Climate change 2013: the physical science basis, in: Stocker, T. F., Qin, D., Plattner, G.-K., Tignor, M., Allen, S. K., Boschung, J., Nauels, A., Xia, Y., Bex, V., and Midgley, P. M. (Eds.): Contribution of working group I to the fifth assessment report of the intergovernmental panel on climate change, Cambridge University Press, Cambridge, United Kingdom and New York, NY, USA, 1535 pp., 2013.

Jansson. A., Norkko, J., Dupont, S., and Norkko, A.: Growth and survival in a changing environment: Combined effects of moderate hypoxia and low pH on juvenile bivalve *Macoma balthica*, J. Sea Res., 102, 41–47, https://doi.org/10.1016/j.seares.2015.04.006, 2015.

Jantzen, C., Laudien, J., Sokol, S., Försterra, G., Häussermann, V., Kupprat, F., and Richter, C.: In situ short-term growth rates of a cold–water coral, Mar. Freshw. Res., 64, 631–641, https://doi.org/10.1071/mf12200, 2013a.

Jantzen, C., Häussermann, V., Försterra, G., Laudien, J., Ardelan, M., Maier, S., and Richter, C.: Occurrence of a cold-water coral along natural pH gradients (Patagonia, Chile), Mar. Biol., 160, 2597–2607, https://doi.org/10.1007/s00227-013-2254-0, 2013b.

Jantzen, C., Laudien, J., Häussermann, V., Försterra, G., and Richter, C.: Seawater carbonate chemistry measured in fjord Comau, Patagonia, Chile (02-2011), Alfred Wegener Institute, Helmholtz Center for Polar and Marine Research, Bremerhaven, PANGAEA, https://doi.org/10.1594/PANGAEA.884131, 2017.

Jope, H. M.: Composition of brachiopod shell, in: Treatise on Invertebrate Paleontology. Part H, Brachiopoda, edited by: Moore, R. C., Geological society of America and University of Kansas Press, New York and Lawrence, 156–164, 1965.

Jurikova, H., Liebetrau, V., Gutjahr, M., Rollion-Bard, C., Hu, M. Y., Krause, S., Henkel, D., Hiebenthal, C., Schmidt, M., Laudien, J., and Eisenhauer, A.: Boron isotope systematics of cultured brachiopods: response to acidification, vital effects and implications for palaeo-pH reconstruction, Geochim. Cosmochim. Ac., accepted, 2019.

Kim, S. T. and O'Neil, J. R.: Equilibrium and nonequilibrium oxygen isotope effects in synthetic carbonates, Geochim. Cosmochim. Ac., 61, 3461–3475, https://doi.org/10.1016/s0016-7037(97)00169-5, 1997.

Krief, S., Hendy, E. J., Fine, M., Yam, R., Meibom, A., Foster, G. L., and Shemesh, A.: Physiological and isotopic responses of scleractinian corals to ocean acidification, Geochim. Cosmochim. Ac., 74, 4988–5001, https://doi.org/10.1016/j.gca.2010.05.023, 2010.

Kurihara, H.: Effects of CO_2-driven ocean acidification on the early developmental stages of invertebrates, Mar. Ecol. Prog. Ser., 373, 274–284, https://doi.org/10.3354/meps07802, 2008.

Laudien, J., Häussermann, V., Försterra, G., and Göhlich, H.: Physical oceanographic profiles of seven CTD casts from Gulf of Ancud into Comau Fjord in 2014, Alfred Wegener Institute, Helmholtz Center for Polar and Marine Research, Bremerhaven, PANGAEA, https://doi.org/10.1594/PANGAEA.832187, 2014.

Liu, W. and He, M.: Effects of ocean acidification on the metabolic rated of three species of bivalve from southern coast of China, Chin. J. Oceanol. Limn., 30, 206–211, https://doi.org/10.1007/s00343-012-1067-1, 2012.

MacKinnon, D. I.: The shell structure in spiriferide brachiopoda, Bull. Br. Mus. Nat. Hist., 5, 189–258, 1974.

MacKinnon, D. I. and Williams, A.: Shell structure of terebratulid brachiopods, Palaeontology, 17, 179–202, 1974.

Marchant, H. K., Calosi, P., and Spicer, J. I.: Short–term exposure to hypercapnia does not compromise feeding, acid–base balance or respiration of *Patella vulgata* but surprisingly is accompanied by radula damage, J. Mar. Biol. Assoc. UK, 90, 1379–1384, https://doi.org/10.1017/s0025315410000457, 2010.

McClintock, J. B., Angus, R. A., Mcdonald, M. R., Amsler, C. D., Catledge, S. A., and Vohra, Y. K.: Rapid dissolution of shells of weakly calcified Antarctic benthic macroorganisms indicates high vulnerability to ocean acidification, Antarct. Sci., 21, 449–456, https://doi.org/10.1017/s0954102009990198, 2009.

McCulloch, M., Trotter, J., Montagna, P., Falter, J., Dunbar, R., Freiwald, A., Försterra, G., Lopez Correa, M., Maier, C., Ruggeberg, A., and Taviani, M.: Resilience of cold–water scleractinian corals to ocean acidification: Boron isotopic systematics of pH and saturation state up–regulation, Geochim. Cosmochim. Ac., 87, 21–34, https://doi.org/10.1016/j.gca.2012.03.027, 2012.

Melzner, F., Stange, P., Trübenbach, K., Thomsen, J., Casties, I., Panknin, U., Gorb, S. N., and Gutowska, M. A.: Food supply and seawater $p\mathrm{CO_2}$ impact calcification and internal shell dissolution in the blue mussel *Mytilus edulis*, PLoS ONE, 6, e24223, https://doi.org/10.1371/journal.pone.0024223, 2011.

Michaelidis, B., Ouzounis, C., Paleras, A., and Pörtner, H. O.: Effects of long-term moderate hypercapnia on acid–base balance and growth rate in marine mussels *Mytilus*

galloprovincialis, Mar. Ecol. Prog. Ser., 293, 109–118, https://doi.org/10.3354/meps293109, 2005.

Mii, H. S. and Grossman, E. L.: Late Pennsylvanian seasonality reflected in the ^{18}O and elemental composition of a brachiopod shell, Geology, 22, 661–664, https://doi.org/10.1130/0091-7613(1994)022<0661:lpsrit>2.3.co;2, 1994.

Mii, H. S., Grossman, E. L., Yancey, T. E., Chuvashov, B., and Egorov, A.: Isotopic records of brachiopod shells from the Russian Platform–evidence for the onset of mid–Carboniferous glaciation, Chem. Geol., 175, 133–147, https://doi.org/10.1016/s0009-2541(00)00366-1, 2001.

Milano, S., Schöne, B. R., Wang, S., and Müller, W. E.: Impact of high pCO$_2$ on shell structure of the bivalve *Cerastoderma edule*, Mar. Environ. Res., 119, 144–155, https://doi.org/10.1016/j.marenvres.2016.06.002, 2016.

Mingliang, Z., Jianguang, F., Jihong, Z., Bin, L., Shengmin, R., Yuze, M., and Yaping, G.: Effect of marine acidification on calcification and respiration of *Chlamys farreri*, J. Shellfish Res., 30, 267–271, https://doi.org/10.2983/035.030.0211, 2011.

Morse, J. W., Arvidson, R. S., and Luttge, A.: Calcium carbonate formation and dissolution, Chem. Rev., 107, 342–381, https://doi.org/10.1002/chin.200719199, 2007.

Movilla, J., Orejas, C., Calvo, E., Gori, A., López Sanz, Á., Grinyó, J., Dominguez–Carrió, C., and Pelejero, C.: Differential response of two Mediterranean cold–water coral species to ocean acidification, Coral Reefs, 33, 675–686, https://doi.org/10.1007/s00338-014-1159-9, 2014.

Navarro, J. M., Torres, R., Acuna, K., Duarte, C., Manriquez, P. H., Lardies, M., Lagos, N. A., Vargas, C., and Aguilera, V.: Impact of medium–term exposure to elevated pCO$_2$ levels on the physiological energetics of the mussel *Mytilus chilensis*, Chemosphere, 90, 1242–1248, https://doi.org/10.1016/j.chemosphere.2012.09.063, 2013.

Nienhuis, S., Palmer, A. R., and Harley, C. D. G.: Elevated CO$_2$ affects shell dissolution rate but not calcification rate in a marine snail, Philos. T. R. Soc. Lon. B, 277, 2553–2558, https://doi.org/10.1098/rspb.2010.0206, 2010.

Orr, J. C., Fabry, V. J., Aumont, O., Bopp, L., Doney, S. C., Feely, R. A., Gnanadesikan, A., Gruber, N., Ishida, A., Joos, F., Key, R. M., Lindsay, K., Maier-Reimer, E., Matear, R., Monfray, P., Mouchet, A., Najjar, R. G., Plattner, G. K., Rodgers, K. B., Sabine, C. L., Sarmiento, J. L., Schlitzer, R., Slater, R. D., Totterdell, I. J., Weirig, M. F., Yamanaka, Y., and Yool, A.: Anthropogenic ocean acidification over the twenty–first century and its impact on calcifying organisms, Nature, 437, 681–686, https://doi.org/10.1038/nature04095, 2005.

Parker, L. M., Ross, P. M., and O'Connor, W. A.: Comparing the effect of elevated pCO$_2$ and temperature on the fertilization and early development of two species of oysters, Mar. Biol., 157, 2435–2452, https://doi.org/10.1007/s00227-010-1508-3, 2010.

Parker, L. M., Ross, P. M., and O'Connor, W. A.: Populations of the Sydney rock oyster, *Saccostrea glomerata*, vary in response to ocean acidification, Mar. Biol., 158, 689–697, https://doi.org/10.1007/s00227-010-1592-4, 2011.

Parker, L. M., Ross, P. M., O'Connor, W. A., Borysko, L., Raftos, D. A., and Pörtner, H.-O.: Adult exposure influences offspring response to ocean acidification in oysters, Glob. Change Biol., 18, 82–92, https://doi.org/10.1111/j.1365-2486.2011.02520.x, 2012.

Parkinson, D., Curry, G. B., Cusack, M., and Fallick, A. E.: Shell structure, patterns and trends of oxygen and carbon stable isotopes in modern brachiopod shells, Chem. Geol., 219, 193–235, https://doi.org/10.1016/j.chemgeo.2005.02.002, 2005.

Payne, J. L. and Clapham, M. E.: End-Permian mass extinction in the oceans: an ancient analog for the twenty-first century?, Annu. Rev. Earth Pl. Sc., 40, 89–111, https://doi.org/10.1146/annurev-earth-042711-105329, 2012.

Peck, L. S., Clarke, A., and Holmes, L. J.: Size, shape and the distribution of organic matter in the Recent Antarctic brachiopod *Liothyrella uva*, Lethaia, 20, 33–40, https://doi.org/10.1111/j.1502-3931.1987.tb00757.x, 1987.

Penman, D. E., Hönisch, B., Rasbury, E. T., Hemming, N. G., and Spero, H. J.: Boron, carbon, and oxygen isotopic composition of brachiopod shells: Intra–shell variability, controls, and potential as a paleo-pH recorder, Chem. Geol., 340, 32–39, https://doi.org/10.1016/j.chemgeo.2012.11.016, 2013.

Pérez-Huerta, A., Cusack, M., McDonald, S., Marone, F., Stampanoni, M., and MacKay, S.: Brachiopod punctae: a complexity in shell biomineralisation, J. Struct. Biol., 167, 62–67, https://doi.org/10.1016/j.jsb.2009.03.013, 2009.

Popov, L. E., Egerquist, E., and Holmer, L. E.: Earliest ontogeny of Middle Ordovician rhynchonelliform brachiopods (Clitambonitoidea and Polytoechioidea): implications for brachiopod phylogeny, Lethaia, 40, 85–96, https://doi.org/10.1111/j.1502-3931.2006.00008.x, 2007.

Popp, B. N., Anderson, T. F., and Sandberg, P. A.: Brachiopods as indicators of original isotopic compositions in some Paleozoic limestones, Geol. Soc. Am. Bull., 97, 1262–1269, https://doi.org/10.1130/0016-7606(1986)97<1262:baiooi>2.0.co;2, 1986.

Range, P., Chícharo, M. A., Ben-Hamadou, R., Piló, D., Matias, D., Joaquim, S., Oliveira, A. P., and Chícharo, L.: Calcification, growth and mortality of juvenile clams *Ruditapes decussatus* under increased pCO$_2$ and reduced pH: Variable responses to ocean acidification at local scales?, J. Exp. Mar. Biol. Ecol., 396, 177–184, https://doi.org/10.1016/j.jembe.2010.10.020, 2011.

Range, P., Piló, D., Ben-Hamadou, R., Chícharo, M. A., Matias, D., Joaquim, S., Oliveira, A. P., and Chícharo, L.: Seawater acidification by CO$_2$ in a coastal lagoon environment: Effects on life history traits of juvenile mussels *Mytilus galloprovincialis*, J. Exp. Mar. Biol. Ecol., 424–425, 89–98, https://doi.org/10.1016/j.jembe.2012.05.010, 2012.

Ries, J. B., Cohen, A. L., and McCorkle, D. C.: Marine calcifiers exhibit mixed responses to CO$_2$-induced ocean acidification, Geology, 37, 1131–1134, https://doi.org/10.1130/g30210a.1, 2009.

Romanin, M., Crippa, G., Ye, F., Brand, U., Bitner, M. A., Gaspard, D., Häussermann, V., and Laudien J.: A sampling strategy for recent and fossil brachiopods: selecting the optimal shell segment for geochemical analyses, Riv. Ital. Paleontol. S., 124, 343–359, 2018.

Shirayama, Y. and Thornton, H.: Effect of increased atmospheric CO$_2$ on shallow water marine benthos, J. Geophys. Res.-Oceans, 110, C09S08, https://doi.org/10.1029/2004jc002618, 2005.

Smirnova, T. N. and Popiel-Barczyk, E.: Characteristics of the shell ultrastructure in Terebratellacea, in: Brachiopods through time, edited by: MacKinnon, D. I., Lee, D. E., and Campbell, J. D. (Eds.): Brachiopods through time, Balkema, Rotterdam, 159–165, 1991.

Steckbauer, A., Ramajo, L., Hendriks, I. R., Fernandez, M., Lagos, N. A., Prado, L., and Duarte, C. M.: Synergistic effects of hypoxia and increasing CO_2 on benthic invertebrates of the central Chilean coast, Front. Mar. Sci., 2, 49, https://doi.org/10.3389/fmars.2015.00049, 2015.

Stemmer, K., Nehrke, G., and Brey, T.: Elevated CO_2 levels do not affect the shell structure of the bivalve *Arctica islandica* from the Western Baltic, PLoS ONE, 8, e70103, https://doi.org/10.1371/journal.pone.0070106, 2013.

Suckling, C. C., Clark, M. M., Richard, J., Morley, S. A., Thorne, M. A., Harper, E. M., and Peck, L. S.: Adult acclimation to combined temperature and pH stressors significantly enhances reproductive outcomes compared to short-term exposures, J. Anim. Ecol., 84, 773–784, https://doi.org/10.1111/1365-2656.12316, 2015.

Takayanagi, H., Asami, R., Abe, O., and Miyajima, T.: Intraspecific variations in carbon-isotope and oxygen-isotope compositions of a brachiopod *Basiliola lucida* collected off Okinawa-jima, southwestern Japan, Geochim. Cosmochim. Ac., 115, 115–136, https://doi.org/10.1016/j.gca.2013.03.026, 2013.

Talmage, S. C. and Gobler, C. J.: Effects of elevated temperature and carbon dioxide on the growth and survival of larvae and juveniles of three species of northwest Atlantic bivalves, PLoS ONE, 6, e26941, https://doi.org/10.1371/journal.pone.0026941, 2011.

Thomsen, J. and Melzner, F.: Moderate seawater acidification does not elicit long-term metabolic depression in the blue mussel *Mytilus edulis*, Mar. Biol., 157, 2667–2676, https://doi.org/10.1007/s00227-010-1527-0, 2010.

Thomsen, J., Gutowska, M. A., Saphörster, J., Heinemann, A., Trübenbach, K., Fietzke, J., Hiebenthal, C., Eisenhauer, A., Körtzinger, A., Wahl, M., and Melzner, F.: Calcifying invertebrates succeed in a naturally CO_2-rich coastal habitat but are threatened by high levels of future acidification, Biogeosciences, 7, 3879–3891, https://doi.org/10.5194/bg-7-3879-2010, 2010.

Tukey, J. W.: Exploratory data analysis, Reading, PA: Addison-Wesley, 1977.

Ullmann, C. V., Frei, R., Korte, C., and Lüter, C.: Element/Ca, C and O isotope ratios in modern brachiopods: Species–specific signals of biomineralization, Chem. Geol., 460, 15–24, https://doi.org/10.1016/j.chemgeo.2017.03.034, 2017.

Watkins, J. M., Nielsen, L. C., Ryerson, F. J., and DePaolo, D. J.: The influence of kinetics on the oxygen isotope composition of calcium carbonate, Earth Planet. Sc. Lett., 375, 349–360, https://doi.org/10.1016/j.epsl.2013.05.054, 2013.

Watson, S., Peck, L. S., Tyler, P. A., Southgate, P. C., Tan, K. S., Day, R. W., and Morley, S. A.: Marine invertebrate skeleton size varies with latitude, temperature and carbonate saturation: implications for global change and ocean acidification, Glob. Change Biol., 18, 3026–3038, https://doi.org/10.1111/j.1365-2486.2012.02755.x, 2012.

Williams, A.: The calcareous shell of the Brachiopoda and its importance to their classification, Biol. Rev., 31, 243–287, https://doi.org/10.1111/j.1469-185x.1956.tb01591.x, 1956.

Williams, A.: Growth and structure of the shell of living articulate brachiopods, Nature, 211, 1146–1148, https://doi.org/10.1038/2111146a0, 1966.

Williams, A.: Evolution of the shell structure of articulate brachiopods, Spec. Pap. Palaeontol., 2, 1–55, 1968.

Williams, A.: The secretion and structural evolution of the shell of thecideidine brachiopods, Philos. T. R. Soc. Lon. B., 264, 439–478, 1973.

Williams, A.: Shell structure, in: Treatise on Invertebrate Paleontology, Part H, Revised, edited by: Kaesler, R. L., Brachiopoda, vol. 1, Geological Society of America Inc., and The University of Kansas, Boulder, Colorado, USA, 267–320, 1997.

Williams, A. and Cusack, M.: Chemicostructural diversity of the brachiopod shell, in: Treatise on Invertebrate Paleontology, Part H, Brachiopoda Revised, edited by: Selden, P. A., vol. 6, Geological Society of America Inc., and The University of Kansas, Boulder, Colorado, USA, 2396–2521, 2007.

Wood, H. L., Spicer, J. I., and Widdicombe, S.: Ocean acidification may increase calcification rates, but at a cost, P. Roy. Soc. Lond. B, Bio., 275, 1767–1773, https://doi.org/10.1098/rspb.2008.0343, 2008.

Yamamoto, K., Asami, R., and Iryu, Y.: Correlative relationships between carbon- and oxygen-isotope records in two cool-temperate brachiopod species off Otsuchi Bay, northeastern Japan, Paleontol. Res., 17, 12–26, https://doi.org/10.2517/1342-8144-17.1.12, 2013.

Ye, F., Crippa, G., Angiolini, L., Brand, U., Capitani, G., Cusack, M., Garbelli, C., Griesshaber, E., Harper, E., and Schmahl, W.: Mapping of recent brachiopod microstructure: a tool for environmental studies, J. Struct. Biol., 201, 221–236, https://doi.org/10.1016/j.jsb.2017.11.011, 2018a.

Ye, F., Crippa, G., Garbelli, C., and Griesshaber, E.: Microstructural data of six recent brachiopod species: SEM, EBSD, morphometric and statistical analyses, Data in Brief, 18, 300–318, https://doi.org/10.1016/j.dib.2018.02.071, 2018b.